Novel deazaflavin analogues potently inhibited tyrosyl DNA phosphodiesterase 2 (TDP2) and strongly sensitized cancer cells toward treatment with topoisomerase II (TOP2) poison etoposide

Jayakanth Kankanala[a,#], Carlos J. A. Ribeiro[a,#], Evgeny Kiselev[b], Azhar Ravji[b], Jessica Williams[a], Jiashu Xie[a], Hideki Aihara[c], Yves Pommier[b], and Zhengqiang Wang[a]

[a)]Center for Drug Design, College of Pharmacy, University of Minnesota, Minneapolis, MN 55455, United States.

[b)]Developmental Therapeutics Branch and Laboratory of Molecular Pharmacology, Center for Cancer Research, National Cancer Institute, National Institutes of Health, Bethesda, MD 20892, United States.

[c)]Department of Biochemistry, Molecular Biology and Biophysics, University of Minnesota, Minneapolis, MN 55455, United States.
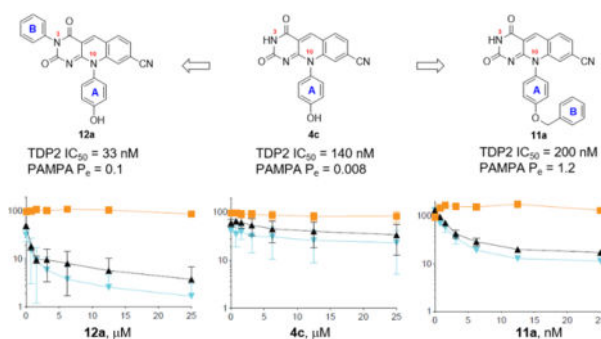
Abstract

Topoisomerase II (TOP2) poisons as anticancer drugs work by trapping TOP2 cleavage complexes (TOP2cc) to generate DNA damage. Repair of such damage by tyrosyl DNA phosphodiesterase 2 (TDP2) could render cancer cells resistant to TOP2 poisons. Inhibiting TDP2 thus represents an attractive mechanism-based chemosensitization approach. Currently known TDP2 inhibitors lack cellular potency and / or permeability. We report herein two novel subtypes of the deazaflavin TDP2 inhibitor core. By introducing an additional phenyl ring to the N-10 phenyl ring (subtype **11**), or to the N-3 site of the deazaflavin scaffold (subtype **12**) we have generated novel analogues with considerably improved biochemical potency and / or permeability. Importantly, many analogues of both subtypes, particularly compounds **11a**, **11e**, **12a**, **12b** and **12h**, exhibited much stronger cancer cell sensitizing effect than the best reported previous analogue **4a** toward the treatment with etoposide (ETP), suggesting that these analogues could serve as effective cellular probes.

Graphical Abstract

Corresponding Author: wangx472@umn.edu; Phone: +1 (612) 626-7025.
[#]These authors contributed equally

TDP2 IC$_{50}$ = 33 nM
PAMPA P$_e$ = 0.1

TDP2 IC$_{50}$ = 140 nM
PAMPA P$_e$ = 0.008

TDP2 IC$_{50}$ = 200 nM
PAMPA P$_e$ = 1.2

Introduction

Topoisomerase II (TOP2) manages DNA topology during essential DNA transactions such as transcription and replication.[1–2] Mechanistically, TOP2 cleaves DNA using its tyrosine residue to generate a transient TOP2 cleavage complexes (TOP2cc) in which TOP2 is covalently linked to the 5′ terminus of the DNA break via a tyrosyl phosphodiester bond. The TOP2cc is typically re-ligated at the end of each catalytic cycle, creating a dynamic DNA equilibrium between the resealed form and the TOP2cc. However, when the normally transient TOP2cc is trapped it becomes abortive and the DNA is damaged. Clinically important TOP2 poisons work by this exact mechanism as they bind to and stabilize the TOP2cc to prevent DNA re-ligation, resulting in the accumulation of abortive TOP2cc.[3–4] Multiple lines of recent evidence demonstrated that tyrosyl DNA phosphodiesterase 2 (TDP2) repairs TOP2-mediated DNA damages, including the abortive TOP2cc trapped by TOP2 poisons, and causes cellular resistance to TOP2 poisons: 1) in cultured cells and animal models the lack of TDP2 led to enhanced cellular sensitivity to DNA breaks induced by TOP2 poisons;[5–9] 2) up-regulation of TDP2 transcription through a gain-of-function p53 mutation was linked to TOP2 poison resistance in human lung cancer.[10] TOP2 poisons, such as etoposide (ETP), teniposide and doxorubicin, are widely used for treating a wide range of cancers, including lung cancer, testicular cancer, breast cancer and as a second line treatment option for platinum-resistant ovarian cancers.[11] Inhibiting TDP2 represents a mechanism-based sensitizing approach which could allow these poisons to be used at lower and safer doses and against cancers that are resistant to TOP2 poisons.

In addition, TDP2 could be involved in the genome repair of certain DNA and RNA viruses, such as hepatitis B virus (HBV)[12] and picornaviruses.[13–14] The genome replication of these viruses is protein-primed via a tyrosine residue, which results in protein tyrosine-nucleic acid adducts similar to the TOP2cc. The repair to remove the viral proteins at the 5′ end of the viral genomes is believed to be carried out by host DNA repair machineries, possibly TDP2. Therefore, inhibiting TDP2 could also represent a novel antiviral approach.

A few compounds have recently been reported as TDP2 inhibitors (Figure 1), including benzopteridine-2,4-dione (**1**, Ro 08–2750),[15] diaminoquinoline-2,8-dione (**2**, NSC111041),[16] isoquinoline-1,3-diones (**3**),[17] deazaflavins (**4**),[15, 18–19] benzylidenepyrazolone (**5**, NSC375976),[20] phenylacetylcystine (**6**, n = 0, NSC114532; n =1, NSC3198),[20] quinazolinylaminopyrimidinone (**7**),[21] triazolopyridine (**8**),[22] indenoisoquinolines (**9**),[23–24]

and furoquinolinediones (**10**)[25] (Figure 1). Most of these inhibitors were identified through random screening of compound libraries using biochemical assays.[26] A few of them, such as **1** (reactive group), **2** (redox cycler), **5** (Michael acceptor), and **6** (redox cycler), fit the profiles of pan-assay interference structure (PAINS)[27] and may not be appropriate for further development as TDP2 inhibitors. Compound **9** was reported as triple inhibitors of TOP1/TDP1/TDP2.[24] More importantly, these compounds generally inhibit TDP2 only moderately with IC_{50} values in micromolar range. The exception is the deazaflavin chemotype (**4**) which inhibited TDP2 in nanomolar range with a genuine structure-activity relationship (SAR)[15] and a defined binding mode,[18] and sensitized cancer cells to TOP2 poison ETP,[19] representing by far the most potent and the best characterized TDP2 inhibitor type. The challenge, however, is that the SAR revealed a strong dependence of TDP2 inhibition on the H-bond donating ability of the substituent on N-10 phenyl, rendering potent compounds poorly permeable.[15] This is consistent with the observation that the sensitizing effect by the most potent analogue **4a** (R = meta-tetrazole, chemotype **4**) on DT40, chicken lymphoma cells, toward ETP treatment was not as pronounced as predicted based on its nanomolar potency in biochemical assays.[19] Therefore, as potent as some of the reported **4** analogues are in biochemical assays, their use as cellular probes to study cellular functions of TDP2 is limited.

Ideally, molecular probes enabling cellular studies should have balanced profiles of potent inhibitory activity, good permeability and low cytotoxicity within the concentration range of studies. Interestingly, Raoof et al. also reported that an inactive compound of the same deazaflavin core exhibited good permeability and reduced efflux,[15] suggesting that it is possible to develop the deazaflavin core into useful probes. We report herein our medicinal chemistry efforts toward this end. By chemically modifying the N-10 and N-3 sites (Figure 2), we have generated novel deazaflavin subtypes with enhanced potency, both biochemically and in cancer cells, and improved permeability.

Results and Discussion

Chemistry

Deazaflavin scaffold **4** was prepared according to reported procedures (Scheme 1A).[15] The synthesis involved reaction of 6-chlorouracil (**13**) with substituted amines (**14**) to provide 6-amino intermediate **15** which upon reacting with 4-cyano-2-fluorobenzaldehyde (**16**) yielded the deazaflavin core (**4**). The key to the synthesis of subtype **11** was the preparation of amine intermediates **20**-**21** (Scheme 1B). Intermediates **20** were synthesized from an *N*-Boc protected 3 or 4-aminophenol (**17**) which was treated with substituted benzyl bromides (**18**) to yield corresponding *O*-benzyl derivatives (**19**). The subsequent deprotection of the *N*-Boc with TFA gave the aniline derivatives (**20**). On the other hand, amine intermediates **21** was synthesized via an S_NAr reaction of phenolic alcohol **22** with 4-nitrophenyl fluoride **23** followed by the reduction of the nitro group. To advance the synthesis, amines **20** or **21** were reacted with 6-chlorouracil (**13**) to give intermediate **25** which upon condensation with 4-cyano-2-fluorobenzaldehyde (**16**) furnished subtype **11** (Scheme 1B).

N3-substituted deazaflavin subtype **12** was efficiently synthesized in one step from scaffold **4** *via* a modified Chan-Lam coupling[28–30] with substituted boronic acids **26** under the catalysis of $Cu(OAc)_2$ (Scheme 1C).

It is important to note that most of our analogues of subtype **12** bear a phenolic alcohol off phenyl ring A, which could complicate their synthesis from the corresponding **4** via the Chan-Lam coupling as both the NH at 3 position and the phenolic alcohol can be arylated under the Chan-Lam condition (Figure 3). However, in all our synthesis the *N*-arylated compounds of subtype **12** were obtained as the sole products, and the formation of the *O*-arylated subtype **11** was not observed (Figure 3). This complete chemoselectivity of *N*-arylation over *O*-arylation[31] under Chan-Lam condition was confirmed by synthesizing analogue **12b, 12j-k** *via* an alternative linear synthesis (Scheme 2). In this synthesis, phenyl ring B was introduced at the very beginning of the synthesis as part of the starting urea **27**. Cyclocondensation of **27** with diethylmalonate produced the 1-phenylpyrimidine-trione (**28**) in excellent yield under reflux which upon treatment with $POCl_3$ in the presence of $BnEt_3NCl$ yielded the key intermediate 3-phenylpyrimidine-2,4-dione (**29**).[32–33] Reaction of 6-chloro intermediate (**29**) with anilines afforded 6-amination products in moderate to excellent yields. The desired deazaflavin subtype **12** was constructed in moderate yields by the subsequent amination and condensation reaction sequence.[15] **12b** synthesized from this linear route was found identical to that obtained via the Chan-Lam coupling. It is also noteworthy that analogues **12j-k** and **31** were synthesized via the linear route only.

Biology

To assess TDP2 inhibitory activity all final compounds were tested in dose-response fashion using our recently developed fluorescence-based biochemical assay.[21] Most analogues were also evaluated for both the toxicity and sensitizing effect on chicken lymphoma DT40 cells toward treatment with ETP. Permeability was measured for all final compounds in Parallel Artificial Membrane Permeation Assay (PAMPA).[34] Additional cytotoxicity studies were carried out in HepG2 cells for all final compounds, and in HeLa cells for most analogues. These cells are widely used for the infection of HBV and picornavirus, respectively.

The first series of compounds (Table 1) served as a control series centered around analogue **4c**. IC_{50} values from our own biochemical assay largely agreed with reported values[15] (Table 1 footnote) and followed similar SAR trends in that 1) potent TDP2 inhibition by deazaflavin subtype **4** generally required a polar substituent with H-bonding ability on phenyl ring A (**4a-c**); removal (**4d**) or etherification (**4e-h**) of the OH group led to activity drop by 2–10 fold; 2) analogues with a *meta* polar group on phenyl ring A demonstrated better potency than those with a *para* polar group (**4b** vs **4c**). Unfortunately, the polar group (OH or tetrazole) critical for target binding also conferred extremely low PAMPA permeability (**4a-c**) with the effective permeability coefficient (P_e) in the range of 0.003–0.01 (a P_e of 1.5 is considered indicative of high permeability). PAMPA permeability was substantially improved upon removal (**4d**) or etherification (**4e-h**) of the polar OH group (Table 1). Notably analogue **4f** was designed to achieve balanced potency and permeability based on the concept of lipophilic H-bond donor.[35] Because the H of the difluoromethoxy group ($-OCHF_2$) is rendered acidic by strong electron-withdrawing O and F atoms,

presumably this functionality could provide the key H-bonding for potency while improving permeability. However, significantly improved TDP2 inhibition was not observed with **4f** when compared with other ether analogues, particularly **4e**. On the other hand, methylation of the 3-NH group (**31** vs **4c**) led to significantly improved permeability (13 fold) with only a moderate loss of inhibitory activity (2 fold).

These observations prompted us to explore more drastic structural modifications over the original deazaflavin inhibitor type **4**. Specifically, we decided to derivatize the polar group on phenyl ring A and / or the NH group at 3 position of the deazaflavin core with a second phenyl ring (ring B, Figure 2). We expected that such derivatization would improve permeability and hypothesized that the added phenyl ring (B) could provide additional interactions with TDP2 to possibly compensate for the loss of the polar interactions. As for the polar group on phenyl A, we chose the OH group (**4b-c**) mainly due to its ability to confer high potency and easy synthetic accessibility.

We first explored the derivatization of the OH group on phenyl ring A. Toward this end, we synthesized a panel of benzyl ethers and phenyl ethers (subtype **11**, Table 2). The most prominent SAR with this series was that benzyl ethers exhibited considerably higher inhibitory potency than the corresponding phenyl ethers (**11a**, $IC_{50} = 0.196$ μM vs **11g**, $IC_{50} = 1.13$ μM; **11b**, $IC_{50} = 1.60$ μM vs **11h**, $IC_{50} > 10$ μM; **11e**, $IC_{50} = 0.153$ μM vs **11j**, $IC_{50} = 0.934$ μM; **11f**, $IC_{50} = 0.131$ μM vs **11k**, $IC_{50} = 0.186$ μM). Particularly intriguing are **11a** and **11e** which inhibited TDP2 with essentially the same potency as **4c** but exhibited drastically improved permeability over **4c** (75 and 150 fold, respectively). Direct comparison between compounds with an ester functionality and a carboxylic acid functionality (**11e** vs **11f**; **11j** vs **11k**) further confirmed that a polar H-bond donor benefits target binding but compromises permeability. These results validate our approach of derivatizing the polar group, particularly the phenolic OH, for balanced potency and permeability. In addition, the two analogues (**11l-m**) synthesized based on the *meta* phenolic analogue **4b** also showed strong TDP2 inhibition and markedly improved permeability, though the IC_{50} values were much higher than **4b** (8–10 fold).

Next, we probed the impacts of introducing phenyl ring B to the N-3 site while retaining the OH group on phenyl A. For this purpose, Chan-Lam products from both **4c** (*para* phenolic OH, **12a-f**) and **4b** (*meta* phenolic OH, **12g-i**) were obtained. Comparing with subtype **11**, analogues of this series all showed considerably better TDP2 inhibition. As far as SAR is concerned, for analogues (**12a-f**) derived from *para* phenolic alcohol **4c**, the R′ group on phenyl ring B or its position of substitution did not significantly impact the inhibitory potency, with all analogues showing 2–4 fold of improved potency over **4c**. Similar level of potency improvement (2–6 fold) was observed with analogues **12g-i** over the *meta* phenolic alcohol **4b**, though the site of Cl substitution (3′ vs 4′) seems to have a more significant impact on potency. Moderate improvement on the permeability (3–13 fold) over **4b-c** was also observed with all analogues of subtype **12**, with the single exception of **12f**. Nevertheless, the N-3 arylation generated a novel deazaflavin subtype with improved TDP2 inhibition and PAMPA permeability.

Finally, with the N-3 arylated with a *para*-chlorophenyl group, we examined the impact of different phenyl ring A substituents for subtype **12** (Table 4). First of all, removing the polar phenolic OH group of ring A resulted in a compound (**12l**) with much reduced inhibitory activity (**12l** vs **12b** /**12g**, Table 4), though the permeability of **12l** was among the best of all compounds tested. Secondly, replacement of the phenolic alcohol by another polar and H-bond enabling NHSO$_2$Me group generated analogues (**12j-k**) showing the highest potency of all compounds tested so far, with IC$_{50}$ values in single digit nM range for both *para* and *meta* substitution (Table 4). Although permeability remains poor for both, the values still reflect a moderate improvement over **4b-c** (3–6 fold). Overall, our data suggest that the N-3 arylation can be a highly productive and desirable modification, and that the resulting subtype **12** represents the most active inhibitor type of TDP2 to date.

High permeability conferred cytotoxicity.—To gauge their potential as probes for cell-based studies, all final compounds were evaluated in two cell lines for cytotoxicity: the HepG2 cells commonly used for HBV infection[36] and the HeLa cells permissible to picornavirus infection[13–14] (Table 5). Overall, a strong correlation between cytotoxicity and PAMPA permeability was observed. For subtypes **4** and **11** no significant cytotoxicity was observed at concentrations up to 100 μM for compounds with a PAMP P$_e$ 0.5, with **4f** being the only exception; whereas compounds with a PAMP P$_e$ > 0.5 all showed cytotoxicity (Table 5). For subtype **12** only analogue **12l** exhibited high permeability, and hence, cytotoxicity. A few other analogues (**12b-c**, **12d**, **12i**) also demonstrated cytotoxicity despite their low permeability, although their extraordinary TDP2 inhibitory potency indicates that cellular testing of these compounds most likely will not require a concentration range close to the CC$_{50}$. Therefore, their potential as molecular probes for cellular studies should not be overlooked.

Novel inhibitors strongly sensitized DT40 cells toward ETP treatment.—The efficacy of TDP2 inhibitors in potentiating the cytotoxic action of TOP2 poison ETP was evaluated in DT40 chicken lymphoma cells.[37] Cell viability was assayed using the ATPlite luminescence assay (PerkinElmer). DT40 cells were treated with combinations of ETP and TDP2 inhibitors.[19] Treatment with only the TDP2 inhibitor was used as control. It is expected that TDP2 inhibition alone should not elicit cytotoxic effect. On the other hand, supplementation with a TDP2 inhibitor should amplify the cytotoxic effect associated with TOP2 poison ETP. Therefore, the decrease of cell viability with increasing concentrations of the TDP2 inhibitor at constant ETP dose would reflects the cooperative interaction of ETP and the TDP2 inhibitor in inducing toxicity. As shown in Figure 3, previously reported deazaflavin analogue **4a** and our compounds **12a** and **12b** were non-cytotoxic up to 25μM. Although showing toxicity at 25 μM, compound **12h** reached plateau in enhancing ETP action at concentrations below 10 μM. As far as subtype **11** is concerned, compounds **11a** and **11e** both showed general cytotoxicity at μM concentrations (see supporting information) which corroborated their cytotoxicity observed in HepG2 and HeLa cells. However, at concentrations much lower than the cytotoxic concentrations (<25 nM), **11a** and **11e** both sensitized DT40 to ETP treatment. This extraordinary sensitizing effect likely reflects their balanced properties between TDP2 inhibition and PAMPA permeability (Table 2). Nevertheless, all analogues of subtypes **11–12** shown in Figure 3 demonstrated stronger

sensitizing effect when compared with **4a**, the best analogue previously reported. The improved sensitizing effect over **4a** was also observed with many other analogues (see supporting information). These results strongly validate analogues of our new subtypes **11–12** as effective cellular probes.

The overall profiles of TDP2 inhibitory activity, permeability and cytotoxicity for selected analogues of subtypes **11–12** are summarized in Table 6. These properties, along with their superior cancer cell sensitizing effects as shown in Figure 3 and supporting information, strongly validate our novel analogues as improved cellular probes over the best previous analogue **4a**.

Molecular modeling

The co-crystal structure[18] of humanized mouse TDP2 catalytic domain bound to **4c** (PDB code: 5J42) elucidated the binding mode and mechanism of inhibition of deazaflavin inhibitors. Key to inhibitor binding is an extensive H-bonding network involving i) the pyrimido-dione ring of deazaflavin and the guanidine group of R266 and R268 ii) the phenolic hydroxyl group and the backbone carbonyl of N264 via water molecule (Figure 4A).[18] The structure also revealed empty spaces within the binding pocket to accommodate an additional phenyl ring in pointed directions (Figure 4B) to generate two novel subtypes: subtype **11** via the *O*-substitution (left arrow, Figure 4B) and subtype **12** via the *N*-substitution (right arrow, Figure 4B). Importantly, representative analogues **11k** and **12b** are both docked nicely into the crystal structure and are predicted to interact extensively with the side chains of R266 and R268 using its nitrogen and carbonyl oxygen atoms within the pyrimido-dione core (Figure 4C–D), a binding feature also observed with compound **4c** (Figure 4A). In addition, the ether linker of **11k** allows the molecule to extend the added phenyl group into the active site and engage with active site residues H226, N264 and H349 of TDP2 using its phenyl substituent, the carboxylate group (Figure 4C). Additional docking with analogues **11a** and **11e** generated similar poses (SI, Figure S1), except that the additional methylene group extends phenyl ring B further to be in closer contact with H349 (pi-pi interaction) and D262 (pi-anion interaction) than phenyl ring B of **11k**. The methyl carboxylate group in **11e** also forms an H-bond with R206. On the other hand, docking of **12b** reveals a water mediated H-bond interaction between the phenolic hydroxyl group and the side chains of N264 and R266 as observed for **4c**. Nevertheless, unique to subtype **12** is that the phenyl ring at N-3 position of pyrimido-dione is oriented parallel to the R268, which could enable cation-π interactions (Figure 4D). Cation-π interactions[38] are considered vital in several physiological processes which could influence biological structures and molecular recognition.[39–40] These interactions are widely observed in protein-protein[41] or protein-ligand[40, 42] and protein-DNA[43] complexes. In the biochemical assay, all analogues with an N-3 aryl group (**12a-i**) showed much improved potency (2–6 fold) over **4c** or **4b**, whereas compound **31** (N-Me analog) lacking the N-3 aryl ring was found to be 2-fold less active over **4c**. These SAR observations strongly reflect the critical binding benefits gained via the predicted cation-π interaction between the N-3 aryl of subtype **12** and the R268 residue of TDP2.

Conclusion

We have generated two novel deazaflavin subtypes (**11** and **12**) as inhibitor types of TDP2. The synthesis of the N-3 aryl subtype featured a chemoselective Chan-Lam coupling. Most analogues of these chemotypes showed improved biochemical potency and / or PAMPA permeability. Many analogues of our new subtypes **11–12**, particularly **11a, 11e, 12a**, **12b** and **12h**, demonstrated stronger cancer cell sensitizing effect than the best previous analogue **4a** toward ETP treatment. Molecular modeling revealed critical binding interactions provided by the added aryl group, particularly the cation-π interaction between the N-3 aryl and the guanidinium head of R268. Further characterization of these improved deazaflavin analogues in expanded human cancer cell lines, including ETP-resistant cell lines, is currently underway and data will be published in due course.

Experimental section

Chemistry.

General procedures.—All commercial chemicals were used as supplied unless otherwise indicated. Flash chromatography was performed on a Teledyne Combiflash RF-200 with RediSep columns (silica) and indicated mobile phase. All moisture sensitive reactions were performed under an inert atmosphere of ultrapure argon with oven-dried glassware. ^{1}H and ^{13}C NMR spectra were recorded on a Varian 600 MHz or Bruker 400 spectrometer. Mass data were acquired on an Agilent 6230 TOF LC/MS spectrometer capable of ESI and APCI ion sources. Analysis of sample purity was performed on a Varian Prepstar SD-1 HPLC system with a Phenomenex Gemini, 5 μm C18 column (250 mm × 4.6 mm). HPLC conditions: solvent A = H_2O, solvent B = MeCN; flow rate = 1.0 mL/min; compounds were eluted with a gradient of 20% MeCN/H_2O to 100% MeCN for 30 min. Purity was determined by total absorbance at 254 nm. All tested compounds have a purity ≥ 97%.

Deazaflavin analogues (**4a-d**) were reported earlier by Raoof et al.[15]

General procedure for the synthesis of deazaflavin derivatives 4, 11, 12j-k, and 31.[15]: To a suspension of **15**, **25**, or **30** (0.1 g, 1.0 eq) in DMF (2 mL) was added 4-cyano-2-fluorobenzaldehyde (**16**, 1.2 eq) and heated by microwave irradiation at 110 °C for 30 minutes. Water (10 mL) was added to the reaction mixture, and the resulting precipitate was filtered, washed with excess water and dried under vacuum. The crude product was purified by combiflash using 0–2% methanol in DCM and the obtained compound was triturated with methanol to furnish the desired compound. Compounds **4** (Scheme 1A), **11** (Scheme 1B), **12j-k** (Scheme 2), and **31** (Scheme 2) were synthesized starting with intermediate **15**, **25**, **30**, and **30** respectively.

10-(3-Hydroxyphenyl)-2,4-dioxo-2,3,4,10-tetrahydropyrimido[4,5-b]quinoline-8-carbonitrile (4b).[15]: Yellow solid, 75% yield; ^{1}H NMR (600 MHz, DMSO-d_6) δ 11.22 (s, 1H), 10.04 (s, 1H), 9.13 (s, 1H), 8.39 (d, J = 8.2 Hz, 1H), 7.87 (dd, J = 8.2, 1.5 Hz, 1H), 7.49 (t, J = 8.0 Hz, 1H), 7.08 (s, 1H), 7.04 (dd, J = 8.2, 1.5 Hz, 1H), 6.86 – 6.77 (m, 2H). HRMS-ESI (+) *m/z* calculated for $C_{18}H_{11}N_4O_3$, 331.0831 [M+H]+; found: 331.0832.

10-(4-Hydroxyphenyl)-2,4-dioxo-2,3,4,10-tetrahydropyrimido[4,5-b]quinoline-8-carbonitrile (4c).[15]: Yellow solid, 68% yield; ^{1}H NMR (600 MHz, DMSO-d_6) δ 11.21 (s, 1H), 10.03 (s, 1H), 9.13 (s, 1H), 8.39 (d, J = 8.2 Hz, 1H), 7.87 (d, J = 8.2 Hz, 1H), 7.20 (d, J = 8.6 Hz, 2H), 7.12 (s, 1H), 7.03 (d, J = 8.6 Hz, 2H). HRMS-ESI (+) *m/z* calculated for $C_{18}H_{11}N_4O_3$, 331.0831 [M+H]+; found: 331.0834.

2,4-Dioxo-10-phenyl-2,3,4,10-tetrahydropyrimido[4,5-b]quinoline-8-carbonitrile (4d).[15]: Yellow solid (70% yield). ^{1}H NMR (600 MHz, DMSO-d_6) δ 11.25 (s, 1H), 9.17 (s, 1H), 8.42 (d, J = 8.2 Hz, 1H), 7.89 (d, J = 8.1 Hz, 1H), 7.72 (t, J = 7.6 Hz, 2H), 7.67 (t, J = 7.4 Hz, 1H), 7.44 (d, J = 7.7 Hz, 2H), 7.00 (s, 1H). HRMS-ESI (+) *m/z* calculated for $C_{18}H_{11}N_4O_2$, 315.0877 [M+H]+; found: 315.0876.

2,4-Dioxo-10-(4-(trifluoromethoxy)phenyl)-2,3,4,10-tetrahydropyrimido[4,5-b]quinoline-8-carbonitrile (4e).: Yellow solid, 72% yield; ^{1}H NMR (600 MHz, DMSO-d_6) δ 11.27 (s, 1H), 9.16 (s, 1H), 8.41 (d, J = 7.8 Hz, 1H), 7.89 (d, J = 7.8 Hz, 1H), 7.71 (d, J = 7.6 Hz, 2H), 7.60 (d, J = 7.5 Hz, 2H), 7.19 (s, 1H). ^{13}C NMR (150 MHz, DMSO-d_6) δ 161.0, 158.7, 155.8, 148.5, 140.9, 140.8, 135.2, 132.1, 130.4, 126.2, 123.3, 122.5, 120.6, 117.8, 117.4, 115.5. HRMS-ESI (+) *m/z* calculated for $C_{19}H_{10}F_3N_4O_3$, 399.0705 [M+H]+; found: 399.0707.

10-(4-(Difluoromethoxy)phenyl)-2,4-dioxo-2,3,4,10-tetrahydropyrimido[4,5-b]quinoline-8-carbonitrile (4f).: Yellow solid, 62% yield; ^{1}H NMR (600 MHz, DMSO-d_6) δ 11.25 (s, 1H), 9.15 (s, 1H), 8.40 (d, J = 8.2 Hz, 1H), 7.89 (dd, J = 8.1, 1.3 Hz, 1H), 7.56 (t, J = 78 Hz, 1H), 7.52 – 7.48 (m, 4H), 7.15 (s, 1H). ^{13}C NMR (150 MHz, DMSO-d_6) δ 161.4, 159.1, 156.2, 151.7, 141.4, 141.2, 133.4, 132.5, 130.3, 126.5, 123.6, 121.0, 120.2, 118.2, 118.1 (t, J = 256.5 Hz), 117.8, 115.8. HRMS-ESI (+) *m/z* calculated for $C_{19}H_{11}F_2N_4O_3$, 381.0799 [M+H]+; found: 381.0800.

10-(Benzo[d][1,3]dioxol-5-yl)-2,4-dioxo-2,3,4,10-tetrahydropyrimido[4,5-b]quinoline-8-carbonitrile (4g).: Yellow solid, 66% yield; ^{1}H NMR (600 MHz, DMSO-d_6) δ 11.24 (s, 1H), 9.14 (s, 1H), 8.39 (d, J = 8.1 Hz, 1H), 7.88 (d, J = 8.1 Hz, 1H), 7.29 (s, 1H), 7.19 (d, J = 8.2 Hz, 1H), 7.04 (d, J = 1.5 Hz, 1H), 6.88 (dd, J = 8.1, 1.6 Hz, 1H), 6.21 (d, J = 1.9 Hz, 2H). ^{13}C NMR (100 MHz, DMSO-d_6) δ 161.3, 159.0, 156.1, 148.5, 148.0, 141.5, 140.9, 132.2, 130.0, 126.2, 123.3, 121.6, 121.1, 117.9, 117.6, 115.6, 109.0, 108.9, 102.0. HRMS-ESI (+) *m/z* calculated for $C_{19}H_{11}N_4O_4$, 359.0780 [M+H]+; found: 359.0783.

10-(2,2-Difluorobenzo[d][1,3]dioxol-5-yl)-2,4-dioxo-2,3,4,10-tetrahydropyrimido[4,5-b]quinoline-8-carbonitrile (4h).: Yellow solid, 73% yield; ^{1}H NMR (600 MHz, DMSO-d_6) δ 11.28 (s, 1H), 9.17 (s, 1H), 8.39 (d, J = 8.2 Hz, 1H), 7.89 (dd, J = 8.1, 1.2 Hz, 1H), 7.71 (d, J = 8.5 Hz, 1H), 7.59 (d, J = 1.9 Hz, 1H), 7.49 (s, 1H), 7.29 (dd, J = 8.5, 2.0 Hz, 1H). ^{13}C NMR (100 MHz, DMSO-d_6) δ 161.2, 159.0, 156.0, 143.7, 143.3, 141.3, 141.2, 132.6, 132.1, 126.5, 124.8, 123.3, 121.3, 117.8, 117.6, 115.8, 111.3, 111.0. HRMS-ESI (+) *m/z* calculated for $C_{19}H_9F_2N_4O_4$, 395.0592 [M+H]+; found: 395.0596.

10-(4-(Benzyloxy)phenyl)-2,4-dioxo-2,3,4,10-tetrahydropyrimido[4,5-b]quinoline-8-carbonitrile (11a).: Yellow solid, 75% yield; ^{1}H NMR (600 MHz, DMSO-d_6) δ 11.23 (s,

1H), 9.14 (s, 1H), 8.39 (d, *J* = 8.2 Hz, 1H), 7.87 (dd, *J* = 8.1, 1.2 Hz, 1H), 7.53 (d, *J* = 7.4 Hz, 2H), 7.44 (t, *J* = 7.5 Hz, 2H), 7.37–7.33 (m, 3H), 7.31 (d, *J* = 9.0 Hz, 2H), 7.12 (s, 1H), 5.23 (s, 2H). ^{13}C NMR (100 MHz, DMSO-*d_6*) δ 161.3, 159.0, 158.8, 156.1, 141.5, 140.8, 136.5, 132.3, 129.3, 129.2, 128.3, 127.84, 127.7, 126.1, 123.4, 120.9, 118.0, 117.6, 116.1, 115.5, 69.6. HRMS-ESI (+) *m/z* calculated for $C_{25}H_{17}N_4O_3$, 421.1301 [M+H]+; found: 421.1303.

10-(4-((4-Chlorobenzyl)oxy)phenyl)-2,4-dioxo-2,3,4,10-tetrahydropyrimido[4,5-b]quinoline-8-carbonitrile (11b).: Yellow solid, 58% yield; ^{1}H NMR (600 MHz, DMSO-*d_6*) δ 11.23 (s, 1H), 9.15 (s, 1H), 8.40 (d, *J* = 8.1 Hz, 1H), 7.88 (d, *J* = 8.1 Hz, 1H), 7.56 (d, *J* = 8.1 Hz, 2H), 7.51 (d, *J* = 8.1 Hz, 2H), 7.37 (d, *J* = 8.4 Hz, 2H), 7.31 (d, *J* = 8.4 Hz, 2H), 7.11 (s, 1H), 5.24 (s, 2H). ^{13}C NMR (100 MHz, DMSO-*d_6*) δ 161.1, 158.8, 158.4, 155.9, 141.3, 140.6, 135.4, 132.2, 132.1, 129.3, 129.2, 128.2, 125.9, 125.1, 123.2, 120.7, 117.8, 117.4, 115.9, 115.3, 68.5. HRMS-ESI (+) *m/z* calculated for $C_{25}H_{16}ClN_4O_3$, 455.0911 [M+H]+; found: 455.0912.

10-(4-((4-Bromobenzyl) oxy) phenyl)-2, 4-dioxo-2, 3, 4, 10-tetrahydropyrimido [4, 5-b] quinoline-8-carbonitrile (11c).: Orange solid, 69% yield; ^{1}H NMR (600 MHz, DMSO-*d_6*) δ 11.23 (s, 1H), 9.15 (s, 1H), 8.40 (d, *J* = 7.5 Hz, 1H), 7.88 (d, *J* = 7.4 Hz, 1H), 7.64 (d, *J* = 7.3 Hz, 2H), 7.50 (d, *J* = 7.2 Hz, 2H), 7.36 (d, *J* = 7.8 Hz, 2H), 7.31 (d, *J* = 7.0 Hz, 2H), 7.11 (s, 1H), 5.22 (s, 2H). ^{13}C NMR (150 MHz, DMSO-*d_6*) δ 161.8, 159.5, 159.1, 156.5, 142.0, 141.4, 141.2, 136.5, 131.6, 130.4, 130.2, 129.8, 129.7, 123.9, 121.4, 118.5, 118.1, 116.8, 116.4, 115.9, 69.2. HRMS-ESI (+) *m/z* calculated for $C_{25}H_{16}BrN_4O_3$, 499.0406 [M+H]+; found: 499.0407.

10-(4-((3-Chlorobenzyl)oxy)phenyl)-2,4-dioxo-2,3,4,10-tetrahydropyrimido[4,5-b]quinolone −8-carbonitrile (11d).: Yellow solid, 52% yield; ^{1}H NMR (600 MHz, DMSO-*d_6*) δ 11.24 (s, 1H), 9.15 (s, 1H), 8.40 (d, *J* = 8.2 Hz, 1H), 7.88 (dd, *J* = 8.2, 1.2 Hz, 1H), 7.61 (s, 1H), 7.52 – 7.44 (m, 3H), 7.37 (d, *J* = 9.0 Hz, 2H), 7.32 (d, *J* = 9.0 Hz, 2H), 7.12 (s, 1H), 5.26 (s, 2H). ^{13}C NMR (100 MHz, DMSO-*d_6*) δ 162.2, 159.9, 159.4, 156.9, 142.4, 141.7, 140.0, 133.8, 133.1, 131.1, 130.2, 128.6, 128.2, 127.1, 126.9, 124.3, 121.7, 118.9, 118.4, 117.0, 116.3, 69.5. HRMS-ESI (+) *m/z* calculated for $C_{25}H_{16}ClN_4O_3$, 455.0911 [M+H]+; found: 455.0915.

Methyl-3-((4-(8-cyano-2,4-dioxo-3,4-dihydropyrimido[4,5-b]quinolin-10(2H)-yl)phenoxy) methyl)benzoate (11e).: Yellow solid. 82% yield; ^{1}H NMR (600 MHz, DMSO-*d_6*) δ 11.23 (s, 1H), 9.14 (s, 1H), 8.40 (d, *J* = 7.4 Hz, 1H), 8.13 (s, 1H), 7.97 (d, *J* = 7.4 Hz, 1H), 7.88 (d, *J* = 7.5 Hz, 1H), 7.82 (d, *J* = 7.4 Hz, 1H), 7.65 – 7.58 (m, 1H), 7.38–7.34 (m, 4H), 7.11 (s, 1H), 5.33 (s, 2H), 3.88 (s, 3H). ^{13}C NMR (100 MHz, DMSO-*d_6*) δ 166.3, 161.7, 159.4, 159.0, 156.5, 142.0, 141.3, 137.8, 132.8, 132.7, 130.1, 129.8, 129.3, 129.0, 128.6, 126.5, 123.8, 121.3, 118.4, 118.0, 116.6, 115.9, 69.3, 52.5. HRMS-ESI (+) *m/z* calculated for $C_{27}H_{19}N_4O_5$, 479.1355 [M+H]+; found: 479.1357.

3-((4-(8-cyano-2,4-dioxo-3,4-dihydropyrimido[4,5-b]quinolin-10(2H)-yl)phenoxy) methyl)benzoic acid (11f).: Yellow solid. 52% yield; ^{1}H NMR (600 MHz, DMSO-*d_6*) δ 13.05 (s, 1H), 11.23 (s, 1H), 9.15 (s, 1H), 8.40 (d, *J* = 8.2 Hz, 1H), 8.11 (s, 1H), 7.95 (d, *J* =

7.7 Hz, 1H), 7.88 (dd, *J* = 8.2, 1.1 Hz, 1H), 7.78 (d, *J* = 7.6 Hz, 1H), 7.58 (t, *J* = 7.6 Hz, 1H), 7.37 (d, *J* = 8.9 Hz, 2H), 7.33 (d, *J* = 9.0 Hz, 2H), 7.12 (s, 1H), 5.31 (s, 2H). ^{13}C NMR (100 MHz, DMSO-*d*$_6$) δ 167.5, 161.9, 159.6, 159.3, 156.7, 142.2, 141.4, 137.7, 132.9, 132.6, 131.5, 130.0, 129.3, 129.0, 126.7, 124.0, 121.5, 118.6, 118.2, 116.8, 116.1, 69.6. HRMS-ESI (+) *m/z* calculated for $C_{26}H_{17}N_4O_5$, 465.1199 [M+H]+; found: 465.1202.

2,4-Dioxo-10-(4-phenoxyphenyl)-2,3,4,10-tetrahydropyrimido[4,5-b]quinoline-8-carbonitrile (11g).: Yellow solid, 79% yield; ^{1}H NMR (600 MHz, DMSO-*d*$_6$) δ 11.25 (s, 1H), 9.15 (s, 1H), 7.89 (d, J = 8.0 Hz, 1H), 7.50 (t, J = 7.8 Hz, 2H), 7.42 (d, J = 8.6 Hz, 2H), 7.26 (t, J = 7.9 Hz, 5H), 7.22 (s, 1H). ^{13}C NMR (150 MHz, DMSO-*d*$_6$) δ 161.4, 159.2, 157.9, 156.3, 155.4, 141.6, 141.1, 132.4, 131.3, 130.3, 130.1, 126.4, 124.5, 123.6, 121.1, 119.9, 119.1, 118.2, 117.8, 115.8. HRMS-ESI (+) *m/z* calculated for $C_{24}H_{15}N_4O_3$, 407.1144 [M+H]+; found: 407.1146.

10-(4-(4-chlorophenoxy)phenyl)-2,4-dioxo-2,3,4,10-tetrahydropyrimido[4,5-b]quinoline-8-carbonitrile (11h).: Yellow solid, 79% yield; ^{1}H NMR (600 MHz, DMSO-*d*$_6$) δ 11.25 (s, 1H), 9.16 (s, 1H), 8.41 (d, *J* = 8.2 Hz, 1H), 7.90 (dd, *J* = 8.2, 1.3 Hz, 1H), 7.57 – 7.50 (m, 2H), 7.50 – 7.40 (m, 2H), 7.32 – 7.28 (m, 4H), 7.24 (s, 1H). ^{13}C NMR (150 MHz, DMSO-*d*$_6$) δ 161.2, 158.9, 157.2, 156.0, 154.2, 141.3, 140.8, 132.2, 131.4, 129.9, 129.8, 128.0, 126.2, 123.4, 121.3, 120.8, 119.1, 117.9, 117.5, 115.5. HRMS-ESI (+) *m/z* calculated for $C_{24}H_{14}ClN_4O_3$, 441.0754 [M+H]+; found: 441.0756.

10-(4-(4-Fluorophenoxy)phenyl)-2,4-dioxo-2,3,4,10-tetrahydropyrimido[4,5-b]quinoline-8-carbonitrile (11i).: Yellow solid, 81% yield; ^{1}H NMR (400 MHz, DMSO-*d*$_6$) δ 11.24 (s, 1H), 9.15 (s, 1H), 8.40 (d, *J* = 8.2 Hz, 1H), 7.89 (dd, *J* = 8.1, 1.2 Hz, 1H), 7.41 (dd, *J* = 9.4, 2.5 Hz, 2H), 7.35–7.31 (m, 4H), 7.25 – 7.20 (m, 3H). ^{13}C NMR (150 MHz, DMSO-*d*$_6$) δ 161.7, 159.8 (d, *J* = 238.5 Hz), 159.4, 158.5, 156.5, 151.6, 141.8, 141.3, 132.7, 131.5, 130.3, 126.7, 123.9, 122.3 (d, *J* = 7.5 Hz), 121.3, 118.9, 118.4, 118.0, 117.2 (d, *J* = 24 Hz), 116.0. HRMS-ESI (+) *m/z* calculated for $C_{24}H_{14}FN_4O_3$, 425.1050 [M+H]+; found: 425.1052.

Methyl-3-(4-(8-cyano-2,4-dioxo-3,4-dihydropyrimido[4,5-b]quinolin-10(2H)-yl)phenoxy)benzoate (11j).: Yellow solid, 75% yield; ^{1}H NMR (600 MHz, DMSO-*d*$_6$) δ 11.25 (s, 1H), 9.15 (s, 1H), 8.40 (d, *J* = 8.1 Hz, 1H), 7.89 (dd, *J* = 8.1, 1.3 Hz, 1H), 7.83 (d, *J* = 7.9 Hz, 1H), 7.73 – 7.68 (m, 1H), 7.65 (t, *J* = 7.9 Hz, 1H), 7.59 – 7.55 (m, 1H), 7.47 – 7.44 (m, 2H), 7.32 (dd, *J* = 9.3, 2.6 Hz, 2H), 7.23 (s, 1H), 3.87 (s, 3H). ^{13}C NMR (100 MHz, DMSO-*d*$_6$) δ 165.3, 161.3, 159.0, 157.1, 156.1, 155.8, 141.4, 140.9, 132.3, 131.8, 131.5, 130.7, 130.1, 126.3, 124.8, 124.4, 123.4, 120.9, 119.6, 119.5, 118.0, 117.6, 115.6, 52.2. HRMS-ESI (+) *m/z* calculated for $C_{26}H_{17}N_4O_5$, 465.1199 [M+H]+; found: 465.1202.

3-(4-(8-Cyano-2,4-dioxo-3,4-dihydropyrimido[4,5-b]quinolin-10(2H)-yl)phenoxy)benzoic acid (11k).: Yellow solid, 67% yield; ^{1}H NMR (400 MHz, DMSO-*d*$_6$) δ 11.25 (s, 1H), 9.15 (s, 1H), 8.41 (d, *J* = 8.2 Hz, 1H), 7.89 (dd, *J* = 8.2, 1.0 Hz, 1H), 7.81 (d, *J* = 7.6 Hz, 1H), 7.72 (s, 1H), 7.61 (t, *J* = 7.9 Hz, 1H), 7.51 (dd, *J* = 7.9, 2.0 Hz, 1H), 7.45 (d, *J* = 8.8 Hz, 2H), 7.31 (d, *J* = 8.8 Hz, 2H), 7.24 (s, 1H). ^{13}C NMR (100 MHz, DMSO-*d*$_6$) δ 166.6, 161.3, 159.0, 157.3, 156.1, 155.5, 141.4, 140.9, 133.5, 132.3, 131.6, 130.4, 130.1, 126.3, 125.0,

123.7, 123.4, 120.9, 119.8, 119.4, 118.0, 117.6, 115.6. HRMS-ESI (+) *m/z* calculated for $C_{25}H_{15}N_4O_5$, 451.1042 [M+H]+; found: 451.1046.

10-(3-(Benzyloxy)phenyl)-2,4-dioxo-2,3,4,10-tetrahydropyrimido[4,5-b]quinoline-8-carbonitrile (11l).: Yellow solid, 81% yield; ^{1}H NMR (600 MHz, DMSO-*d6*) δ 11.25 (s, 1H), 9.16 (s, 1H), 8.40 (d, *J* = 8.1 Hz, 1H), 7.88 (d, *J* = 8.0 Hz, 1H), 7.63 (t, *J* = 8.0 Hz, 1H), 7.48 (d, *J* = 7.3 Hz, 2H), 7.40 (t, *J* = 7.3 Hz, 2H), 7.36 – 7.28 (m, 2H), 7.16 (s, 1H), 7.05 (s, 1H), 7.01 (d, *J* = 7.5 Hz, 1H), 5.15 (s, 2H). ^{13}C NMR (100 MHz, DMSO-*d6*) δ 161.3, 159.6, 158.6, 156.1, 141.0, 140.9, 137.7, 136.3, 132.3, 131.1, 128.3, 127.8, 126.2, 123.4, 120.8, 120.3, 118.0, 117.6, 116.1, 115.6, 114.7, 69.5. HRMS-ESI (+) *m/z* calculated for $C_{25}H_{17}N_4O_3$, 421.1301 [M+H]+; found: 421.1305.

2,4-Dioxo-10-(3-phenoxyphenyl)-2,3,4,10-tetrahydropyrimido[4,5-b]quinoline-8-carbonitrile (11m).: Yellow solid, 71% yield; ^{1}H NMR (600 MHz, DMSO-*d6*) δ 11.24 (s, 1H), 9.13 (s, 1H), 8.39 (d, *J* = 8.1 Hz, 1H), 7.89 (d, *J* = 8.1 Hz, 1H), 7.70 (t, *J* = 8.1 Hz, 1H), 7.43 (t, *J* = 7.7 Hz, 2H), 7.26 (d, *J* = 9.1 Hz, 2H), 7.23 – 7.15 (m, 5H). ^{13}C NMR (150 MHz, DMSO-*d6*) δ 161.3, 158.7, 158.2, 156.1, 155.7, 141.0, 140.9, 137.9, 132.3, 131.6, 130.1, 126.3, 124.0, 123.5, 122.9, 120.9, 119.2, 119.1, 118.2, 118.1, 117.7, 115.7. HRMS-ESI (+) *m/z* calculated for $C_{24}H_{15}N_4O_3$, 407.1144 [M+H]+; found: 407.1148.

N-(4-(3-(4-chlorophenyl)-8-cyano-2,4-dioxo-3,4-dihydropyrimido[4,5-b]quinolin-10(2H)-yl)phenyl)methanesulfonamide (12j).: Compound **12j** was synthesized using the general procedure described using compound **4a** with **27q** as a starting material. Yellow solid, 43% yield; ^{1}H NMR (600 MHz, DMSO-*d6*) δ 10.28 (s, 1H), 9.26 (s, 1H), 8.47 (d, *J* = 8.2 Hz, 1H), 7.92 (dd, *J* = 8.2, 1.2 Hz, 1H), 7.56 – 7.52 (m, 2H), 7.49 (d, *J* = 8.8 Hz, 2H), 7.41 (d, *J* = 8.8 Hz, 2H), 7.30 – 7.26 (m, 2H), 7.25 (s, 1H), 3.20 (s, 3H). ^{13}C NMR (150 MHz, DMSO-*d6*) δ 161.4, 158.4, 155.5, 142.6, 141.8, 140.2, 135.7, 133.0, 132.9, 131.7, 131.0, 129.8, 129.3, 127.1, 124.1, 121.7, 120.4, 118.4, 118.2, 116.5, 40.5. HRMS-ESI (+) *m/z* calculated for $C_{25}H_{17}ClN_5O_4S$, 518.0690 [M+H]+; found: 518.0694.

N-(3-(3-(4-Chlorophenyl)-8-cyano-2,4-dioxo-3,4-dihydropyrimido[4,5-b]quinolin-10(2H)-yl)phenyl)methanesulfonamide (12k).: Compound **23p** was synthesized using the procedure described for compound **4a** with **27p** as a starting material. Yellow solid, 52% yield; ^{1}H NMR (600 MHz, DMSO-*d6*) δ 10.22 (s, 1H), 9.26 (s, 1H), 8.47 (d, *J* = 8.2 Hz, 1H), 7.92 (dd, *J* = 8.1, 1.4 Hz, 1H), 7.68 (t, *J* = 8.1 Hz, 1H), 7.57 – 7.51 (m, 2H), 7.46 (dd, *J* = 8.3, 1.4 Hz, 1H), 7.31–7.29 (m, 2H), 7.28 (d, *J* = 2.1 Hz, 1H), 7.27 (t, *J* = 2.1 Hz, 1H), 7.19 – 7.16 (m, 1H), 3.12 (s, 3H). ^{13}C NMR (150 MHz, DMSO-*d6*) δ 161.3, 158.1, 155.5, 142.6, 141.5, 140.9, 137.7, 135.7, 133.0, 132.9, 131.8, 131.0, 129.3, 127.2, 124.1, 123.5, 121.7, 120.8, 118.7, 118.5, 118.1, 116.6, 40.5. HRMS-ESI (+) *m/z* calculated for $C_{25}H_{17}ClN_5O_4S$, 518.0690 [M+H]+; found: 518.0691.

10-(4-Hydroxyphenyl)-3-methyl-2,4-dioxo-2,3,4,10-tetrahydropyrimido[4,5-b]quinoline-8-carbonitrile (31).: Yellow solid, 81% yield; ^{1}H NMR (400 MHz, DMSO-*d6*) δ 10.04 (s, 1H), 9.19 (s, 1H), 8.43 (d, *J* = 8.1 Hz, 1H), 7.88 (dd, *J* = 8.1, 1.2 Hz, 1H), 7.19 (d, *J* = 8.7 Hz, 2H), 7.15 (s, 1H), 7.03 (d, *J* = 8.7 Hz, 2H), 3.22 (s, 3H). ^{13}C NMR (150 MHz, DMSO-*d6*) δ 160.7, 158.0, 157.3, 155.5, 141.4, 141.3, 132.2, 129.0, 127.1, 125.9, 123.3, 120.8,

117.5, 117.2, 116.5, 115.4, 27.2. HRMS-ESI (+) *m/z* calculated for $C_{19}H_{13}N_4O_3$, 345.0988 [M+H]+; found: 345.0991.

General procedure for the synthesis of deazaflavin derivatives 12 a-i.: To a suspension of compound **4b** or **4c** (0.1 g, 1.0 eq) in DMF (2 mL) was added phenylboronic acid derivative **26** (3.0 eq), Cu(OAc)$_2$ (0.06 g, 0.30 mmol, 1.0 eq) and stirred at room temperature under air. The reaction was continued until the disappearance of starting material (typically between 24–48 h) and water (10 mL) was added to it. The resulting solution was extracted with EtOAc (3 × 20 mL), washed with brine and evaporated *in vacuo* to leave the crude product. The crude product was purified using Combi flash with 0–100% EtOAc in hexane as an eluent to furnish the desired product.

10-(4-Hydroxyphenyl)-2,4-dioxo-3-phenyl-2,3,4,10-tetrahydropyrimido[4,5-b]quinoline-8-carbonitrile (12a).[44]: Pale yellow solid, 56% yield. ^{1}H NMR (400 MHz, DMSO-*d₆*) δ 10.06 (s, 1H), 9.23 (s, 1H), 8.45 (d, *J* = 8.2 Hz, 1H), 7.90 (dd, *J* = 8.2, 1.1 Hz, 1H), 7.47 (t, *J* = 7.5 Hz, 2H), 7.40 (t, *J* = 7.5 Hz, 1H), 7.26–7.22 (m, 4H), 7.19 (s, 1H), 7.05 (d, *J* = 8.7 Hz, 2H). ^{13}C NMR (150 MHz, DMSO-*d₆*) δ 161.1, 158.4, 158.1, 155.4, 142.0, 141.8, 136.5, 132.6, 129.4, 128.9, 128.7, 127.9, 127.5, 126.4, 123.7, 121.3, 118.2, 117.8, 116.9, 115.9. HRMS-ESI (+) *m/z* calculated for $C_{24}H_{15}N_4O_3$, 407.1144 [M+H]+; found: 407.1146.

3-(4-Chlorophenyl)-10-(4-hydroxyphenyl)-2,4-dioxo-2,3,4,10-tetrahydropyrimido[4,5-b]quinoline-8-carbonitrile (12b).: Yellow solid, 80% yield; ^{1}H NMR (600 MHz, DMSO-*d₆*) δ 10.08 (s, 1H), 9.25 (s, 1H), 8.46 (d, *J* = 8.1 Hz, 1H), 7.91 (d, *J* = 8.2 Hz, 1H), 7.54 (d, *J* = 8.5 Hz, 2H), 7.29 (d, *J* = 8.5 Hz, 2H), 7.23 (d, *J* = 8.6 Hz, 2H), 7.20 (s, 1H), 7.05 (d, *J* = 8.6 Hz, 2H). ^{13}C NMR (150 MHz, DMSO-*d₆*) δ 161.0, 158.4, 158.1, 155.2, 142.0, 141.8, 135.4, 132.6, 132.5, 130.6, 129.3, 128.9, 127.4, 126.5, 123.7, 121.3, 118.1, 117.8, 116.8, 116.0. HRMS-ESI (+) *m/z* calculated for $C_{24}H_{14}ClN_4O_3$, 441.0754 [M+H]+; found: 441.0756.

3-(4-Fluorophenyl)-10-(4-hydroxyphenyl)-2,4-dioxo-2,3,4,10-tetrahydropyrimido[4,5-b]quinoline-8-carbonitrile (12c).: Yellow solid, 30% yield; ^{1}H NMR (600 MHz, DMSO-*d₆*) δ 10.09 (s, 1H), 9.24 (s, 1H), 8.46 (d, *J* = 8.2 Hz, 1H), 7.91 (d, *J* = 8.2 Hz, 1H), 7.33 – 7.27 (m, 4H), 7.24 (d, *J* = 8.6 Hz, 2H), 7.20 (s, 1H), 7.05 (d, *J* = 8.6 Hz, 2H). HRMS-ESI (+) *m/z* calculated for $C_{24}H_{14}FN_4O_3$, 425.1050 [M+H]+; found: 425.1051.

3-(4-Bromophenyl)-10-(4-hydroxyphenyl)-2,4-dioxo-2,3,4,10-tetrahydropyrimido[4,5-b]quinoline-8-carbonitrile (12d).: Yellow solid, 52% yield; ^{1}H NMR (600 MHz, DMSO-*d₆*) δ 10.08 (s, 1H), 9.24 (s, 1H), 8.46 (d, *J* = 8.2 Hz, 1H), 7.91 (dd, *J* = 8.2, 1.2 Hz, 1H), 7.73 – 7.63 (m, 2H), 7.25 – 7.21 (m, 4H), 7.20 (s, 1H), 7.06 – 7.03 (m, 2H). ^{13}C NMR (150 MHz, DMSO-*d₆*) δ 161.7, 159.1, 158.8, 155.8, 142.5, 136.5, 133.4, 132.7, 131.8, 131.5, 130.2, 129.9, 128.1, 127.2, 124.4, 121.7, 118.8, 118.5, 117.7, 116.7. HRMS-ESI (+) *m/z* calculated for $C_{24}H_{14}BrN_4O_3$, 485.0249 [M+H]+; found: 485.0250.

Methyl-3-(8-cyano-10-(4-hydroxyphenyl)-2,4-dioxo-4,10-dihydropyrimido[4,5-b]quinolin-3(2H)-yl)benzoate (12e).: Yellow solid, 59% yield; ^{1}H NMR (600 MHz, DMSO-*d₆*) δ 10.09 (s, 1H), 9.24 (s, 1H), 8.47 (d, *J* = 7.8 Hz, 1H), 7.99 (d, *J* = 7.4 Hz, 1H), 7.92 (d, *J* = 7.6 Hz, 1H), 7.85 (s, 1H), 7.64 (t, *J* = 7.4 Hz, 1H), 7.55 (d, *J* = 6.8 Hz, 1H), 7.29 – 7.18

(m, 3H), 7.06 (d, J = 7.8 Hz, 2H), 3.87 (s, 3H). ^{13}C NMR (150 MHz, DMSO-d_6) δ 165.9, 161.4, 158.6, 158.4, 155.6, 142.2, 142.0, 137.2, 134.0, 132.9, 130.7, 129.8, 129.8, 129.6, 128.9, 127.7, 126.8, 123.9, 121.6, 118.4, 118.1, 117.1, 116.2, 52.6. HRMS-ESI (+) m/z calculated for $C_{26}H_{17}N_4O_5$, 465.1199 [M+H]+; found: 465.1199.

3-(8-cyano-10-(4-hydroxyphenyl)-2,4-dioxo-4,10-dihydropyrimido[4,5-b]quinolin-3(2H)-yl)benzamide (12f).: Yellow solid, 72% yield; ^{1}H NMR (600 MHz, DMSO-d_6) δ 10.08 (s, 1H), 9.26 (s, 1H), 8.47 (d, J = 8.2 Hz, 1H), 8.02 (s, 1H), 7.91 (d, J = 8.1 Hz, 2H), 7.74 (s, 1H), 7.56 (t, J = 7.8 Hz, 1H), 7.44 – 7.39 (m, 2H), 7.25 (d, J = 8.7 Hz, 2H), 7.20 (s, 1H), 7.05 (d, J = 8.7 Hz, 2H). ^{13}C NMR (150 MHz, DMSO-d_6) δ 167.3, 161.3, 158.6, 158.3, 155.5, 142.3, 142.0, 136.7, 135.3, 132.8, 131.8, 129.6, 129.1, 128.2, 127.7, 127.1, 126.7, 123.9, 121.6, 118.3, 118.0, 117.1, 116.2. HRMS-ESI (+) m/z calculated for $C_{25}H_{16}N_5O_4$, 450.1202 [M+H]+; found: 450.1202.

3-(4-Chlorophenyl)-10-(3-hydroxyphenyl)-2,4-dioxo-2,3,4,10-tetrahydropyrimido[4,5-b]quinoline-8-carbonitrile (12g).: Yellow solid, 65% yield; ^{1}H NMR (600 MHz, DMSO-d_6) δ 10.09 (s, 1H), 9.26 (s, 1H), 8.47 (d, J = 8.2 Hz, 1H), 7.92 (dd, J = 8.2, 1.2 Hz, 1H), 7.56 – 7.50 (m, 3H), 7.29 (d, J = 8.6 Hz, 2H), 7.17 (s, 1H), 7.07 (dd, J = 8.2, 1.7 Hz, 1H), 6.86 (d, J = 7.8 Hz, 1H), 6.83 (d, J = 2.0 Hz, 1H). ^{13}C NMR (100 MHz, DMSO-d_6) δ 160.8, 158.9, 157.4, 155.0, 141.9, 140.9, 137.2, 135.2, 132.4, 132.3, 131.1, 130.4, 128.7, 126.3, 123.4, 121.0, 118.2, 117.9, 117.6, 116.8, 115.8, 115.0. HRMS-ESI (+) m/z calculated for $C_{24}H_{14}ClN_4O_3$, 441.0754 [M+H]+; found: 441.0749.

3-(3-Chlorophenyl)-10-(3-hydroxyphenyl)-2,4-dioxo-2,3,4,10-tetrahydropyrimido[4,5-b]quinoline-8-carbonitrile (12h).: Yellow solid, 51% yield; ^{1}H NMR (600 MHz, DMSO-d_6) δ 10.09 (s, 1H), 9.26 (s, 1H), 8.48 (d, J = 8.2 Hz, 1H), 7.92 (dd, J = 8.1, 1.3 Hz, 1H), 7.54 – 7.48 (m, 3H), 7.40 (t, J = 1.8 Hz, 1H), 7.25 (dt, J = 7.4, 1.6 Hz, 1H), 7.18 (s, 1H), 7.07 (dd, J = 8.3, 1.7 Hz, 1H), 6.87 – 6.84 (m, 1H), 6.83 (t, J = 2.1 Hz, 1H). ^{13}C NMR (100 MHz, DMSO-d_6) δ 160.8, 158.9, 157.4, 155.0, 141.9, 140.9, 137.2, 135.2, 132.4, 132.3, 131.1, 130.4, 128.7, 126.3, 123.4, 121.0, 118.2, 117.9, 117.6, 116.8, 115.8, 115.0. HRMS-ESI (+) m/z calculated for $C_{24}H_{14}ClN_4O_3$, 441.0754 [M+H]+; found: 441.0755.

3-(3,4-Dichlorophenyl)-10-(3-hydroxyphenyl)-2,4-dioxo-2,3,4,10-tetrahydropyrimido[4,5-b]quinoline-8-carbonitrile (12i).: Yellow solid, 48% yield; ^{1}H NMR (600 MHz, DMSO-d_6) δ 10.11 (s, 1H), 9.28 (s, 1H), 8.49 (d, J = 8.2 Hz, 1H), 7.94 (dd, J = 8.2, 1.5 Hz, 1H), 7.77 (d, J = 8.5 Hz, 1H), 7.65 (d, J = 2.3 Hz, 1H), 7.52 (t, J = 8.0 Hz, 1H), 7.32 (dd, J = 8.5, 2.3 Hz, 1H), 7.19 (s, 1H), 7.07 (dd, J = 8.2, 1.5 Hz, 1H), 6.91 – 6.78 (m, 2H). ^{13}C NMR (100 MHz, DMSO-d_6) δ 161.5, 159.7, 158.2, 155.5, 142.8, 141.7, 138.0, 137.1, 133.2, 131.9, 131.7, 131.5, 131.4, 130.0, 127.3, 124.2, 121.9, 119.0, 118.6, 118.4, 117.6, 116.7, 115.8. HRMS-ESI (+) m/z calculated for $C_{24}H_{13}Cl_2N_4O_3$, 475.0365 [M+H]+; found: 475.0367.

Biology

14M_zTDP2 fluorescence-based biochemical assay—The reaction buffer used was composed of 50 mM Tris-HCl pH 7.4, 10 mM $MgCl_2$, 80 mM KCl, 0.05 % (v/v) Tween-20, and 1 mM DTT. To a black 384-well plate, 10 μL of compound solution (in reaction buffer,

concentration 2-fold higher than the tested concentration, final DMSO concentration of 2.5 %) was added, followed by addition of 5 μL of 14M_TDP2 enzyme (25 pM, final concentration of 6.25 pM). After a pre-incubation period of 10 minutes, 5 μL of substrate 5'-(6-FAM-NHS)(5'-tyrosine)GATCT(3'-BHQ-1)-3' (4 μM, final concentration of 1 μM) was added, and the reaction was allowed to proceed at 25 °C for 60 minutes. The fluorescence of the product was measured using a SpectraMax M5e (Molecular Devices) (λex 285 nm; λem 325 nm; λcutoff 315nm) in kinetic-mode at 25 °C for 60 minutes.[21] IC_{50} experiments data using 12 concentrations of inhibitor (2-fold dilutions) and vehicle-alone were fitted by GraphPad Prism software. IC_{50} determinations represent the means of three independent experiments performed in triplicate.

Sensitizing assay in DT40 cells—Drug cellular sensitivity was measured as previously described.[19] Cells were continuously exposed to various drug concentrations for 72 h. Fifteen hundred DT40 cells/well were seeded into a 96-well white plate (PerkinElmer) and treated with drugs as single agents or in combination in 150 μL of medium. Cell viability was determined at 72 h by adding 75 μL of ATPlite solution (ATPlite 1-step kit, PerkinElmer). After 15 min incubation, luminescence was measured on an EnVision Plate Reader (PerkinElmer). The ATP level in untreated cells was defined as 100%, and viability of treated cells was defined as ATP level of treated cell/ATP level of untreated cells × 100.

Parallel artificial membrane permeability assay (PAMPA)—The membrane permeability of selected compounds were evaluated using the Corning Gentest Pre-coated PAMPA Plate System (Cat. No. 353015). The pre-coated plate assembly, which was stored at −20°C, was taken to thaw for 30 min at room temperature. The permeability assay was carried out in accordance with the manufacturer's protocol. In summary, the 96-well filter plate, pre-coated with lipids, was used as the permeation acceptor and a matching 96 well receiver plate was used as the permeation donor. Compound solutions were prepared by diluting 10 mM DMSO stock solutions in DPBS to a final concentration of 10 μM. The compound solutions were added to the wells (300 μL/well) of the receiver plate and DPBS was added to the wells (200 μL/well) of the pre-coated filter plate. The filter plate was then coupled with the receiver plate and the plate assembly was incubated at 25 °C without agitation for five hours. At the end of the incubation, the plates were separated and the final concentrations of compounds in both donor wells and acceptor wells were analyzed using LC-MS/MS. Permeability of the compounds were calculated using the following formula $Pe = \{-\ln[1-CA(t)/Ceq]\}/[A×(1/VD+1/VA)×t]$, where A = filter area (0.3 cm^2), V_D = donor well volume (0.3 mL), V_A = acceptor well volume (0.2 mL), t = incubation time (seconds), $C_A(t)$ = compound concentration in acceptor well at time t, $C_D(t)$ = compound concentration in donor well at time t, and $C_{eq} = [C_D(t)×V_D+C_A(t)×V_A]/(V_D+V_A)$. A cutoff criterion of Pe value at $1.5 × 10^{-6}$ cm/s was used to classify the compounds into high and low permeability according to the literature report of this PAMPA plate system.[45]

MTT cytotoxicity assay—Hep G2 cells (human liver carcinoma) were maintained in growth media: DMEM:F12 supplemented with 10% fetal bovine serum and 1% penicillin/streptomycin (Invitrogen). HeLa cells (human cervical adenocarcinoma) were maintained in growth media: DMEM supplemented with 10% fetal bovine serum and 1% penicillin/

streptomycin (Invitrogen). Cells were plated in 96-well plates at $1 - 2.5 \times 10^4$ cells per well in growth media. Compounds were added to the plate in 3-fold dilution made in DMSO, starting at 20 mM, and 1 μL of compound solution was added to each well. The final volume in each well was 200 μL, yielding a final DMSO concentration of 0.5%. Compounds were tested at 9, 3x dilutions from 100 uM final concentration in growth media. Control wells contained 0.5% DMSO (positive control) or 50% DMSO (negative control) and all reactions were done in triplicate. The plate was incubated for 72 h at 37 °C in a 5% CO_2/ 95% air humidified atmosphere. Measurement of cell viability was carried out using a modified method of Mosmann[46] based on 3-(4,5-dimethylthiazol-2-yl)-2,5-diphenyltetrazolium bromide (MTT). MTT was prepared fresh at 1 mg/mL in serum-free, phenol red-free RPMI 1640 media. MTT solution (200 μL) was added to each well, and the plate was incubated as described above for 3 h. The MTT solution was removed, and the formazan crystals were solubilized with 200 μL of isopropanol. The plate was read on a SpectraMax i3 spectrophotometer (Molecular Devices) at 570 nm for formazan and 650 nm for background subtraction. CC_{50} values were calculated by fitting the data in GraphPad Prism software.

Molecular modeling and docking analysis

Molecular modeling was performed using the Schrodinger small molecule drug discovery suite 2015–4.[47] The crystal structure of catalytic domain of humanized mouse TDP2 in complex with **4c** as reported by Hornyak et.al[18] was retrieved from the protein data bank (PDB code: 5J42). The above structure was analyzed using Maestro[48] (Schrodinger Inc.[49]) and subjected to docking protocol which involves several steps including preparing protein of interest, grid generation, ligand preparation and docking. The crystal structure was refined using protein preparation wizard[48] (Schrodinger Inc.[49]) in which missing hydrogen atoms and side chains were added and minimized using OPLS 2005 force field[50] to optimize hydrogen bonding network and converge the heavy atoms to an rmsd of 0.3 Å. In the processed crystal structure, the two chains (A & B) were separated and analyzed separately. In both chains, **4c** forms a key hydrogen bond interaction between the nitrogen of pyrimido-dione ring and the side chain of R276 (R266_hTDP2). The side chain of R241 (R231_hTDP2) was positioned to make a π - π interaction with the face of the tricyclic core of **4c** and the phenolic hydroxyl group of **4c** was observed to make water mediated interaction with the catalytic side chain of N274 (N264_hTDP2). The tricyclic core of deazaflavin extends in to a hydrophobic pocket lined by W307 (W297_hTDP2), L323 (L313_hTDP2) and F325 (F315_hTDP2). Chain B was chosen for further docking analysis. The receptor grid generation tool in Maestro (Schrodinger Inc.)[51] was used to define an active site around the native ligand (**4c**) to cover all the residues within 12 Å. All the compounds were drawn using Maestro and subjected to Lig Prep[52] to generate conformers, possible protonation at pH of 7±3 that serves as an input for docking process. All the dockings were performed using Glide XP[53] (Glide[54], version 6.9) with the van der Waals radii of nonpolar atoms for each of the ligands were scaled by a factor of 0.8. The solutions were further refined by post docking and minimization under implicit solvent to account for protein flexibility. The residue numbers of TDP2 used in the discussion and the figures were based on the human TDP2.

Supplementary Material

Refer to Web version on PubMed Central for supplementary material.

ACKNOWLEDGMENTS

ABBREVIATIONS USED

|	
TOP2	topoisomerase II
TOP2cc	TOP2 cleavage complex
TDP2	tyrosyl DNA phosphodiesterase 2
ETP	etoposide
HBV	hepatitis B virus
SAR	structure-activity-relationship
PAMPA	Parallel Artificial Membrane Permeation Assay

References

1. Pommier Y; Sung YL; Huang SYN; Nitiss JL, Roles of Eukaryotic Topoisomerases in Transcription, Replication and Genomic Stability. Nat. Rev. Mol. Cell. Bio 2016, 17, 703–721. [PubMed: 27649880]

2. Nitiss JL, DNA Topoisomerase II and Its Growing Repertoire of Biological Functions. Nat. Rev. Cancer 2009, 9, 327–337. [PubMed: 19377505]

3. Pommier Y, Drugging Topoisomerases: Lessons and Challenges. ACS. Chem. Biol 2013, 8, 82–95. [PubMed: 23259582]

4. Pommier Y; Leo E; Zhang HL; Marchand C, DNA Topoisomerases and Their Poisoning by Anticancer and Antibacterial Drugs. Chem. Biol 2010, 17, 421–433. [PubMed: 20534341]

5. Gomez-Herreros F; Romero-Granados R; Zeng ZH; Alvarez-Quilon A; Quintero C; Ju LM; Umans L; Vermeire L; Huylebroeck D; Caldecott KW; Cortes-Ledesma F, Tdp2-Dependent Non-Homologous End-Joining Protects against Topoisomerase II-Induced DNA Breaks and Genome Instability in Cells and in Vivo. PLOS Genet. 2013, 9.

6. Gomez-Herreros F; Schuurs-Hoeijmakers JHM; McCormack M; Greally MT; Rultenl S; Romero-Granados R; Counihan TJ; Chaila E; Conroy J; Ennis S; Delanty N; Cortes-Ledesma F; de Brouwer APM; Cavallerit GL; El-Khamisy SF; de Vries BBA; Caldecott KW, Tdp2 Protects Transcription from Abortive Topoisomerase Activity and Is Required for Normal Neural Function. Nat. Genet 2014, 46, 516–521. [PubMed: 24658003]

7. Ledesma FC; El Khamisy SF; Zuma MC; Osborn K; Caldecott KW, A Human 5 '-Tyrosyl DNA Phosphodiesterase That Repairs Topoisomerase-Mediated DNA Damage. Nature 2009, 461, 674–678. [PubMed: 19794497]

8. Zeng ZH; Cortes-Ledesma F; El Khamisy SF; Caldecott KW, Tdp2/Ttrap Is the Major 5 '-Tyrosyl DNA Phosphodiesterase Activity in Vertebrate Cells and Is Critical for Cellular Resistance to Topoisomerase II-Induced DNA Damage. J. Biol. Chem 2011, 286, 403–409. [PubMed: 21030584]

9. Maede Y; Shimizu H; Fukushima T; Kogame T; Nakamura T; Miki T; Takeda S; Pommier Y; Murai J, Differential and Common DNA Repair Pathways for Topoisomerase I- and II-Targeted Drugs in a Genetic Dt40 Repair Cell Screen Panel. Mol. Cancer Ther 2014, 13, 214–220. [PubMed: 24130054]

10. Do PM; Varanasi L; Fan SQ; Li CY; Kubacka I; Newman V; Chauhan K; Daniels SR; Boccetta M; Garrett MR; Li RZ; Martinez LA, Mutant P53 Cooperates with Ets2 to Promote Etoposide Resistance. Gene Dev. 2012, 26, 830–845. [PubMed: 22508727]

11. Nitiss JL, Targeting DNA Topoisomerase II in Cancer Chemotherapy. Nat. Rev. Cancer 2009, 9, 338–350. [PubMed: 19377506]

12. Koniger C; Wingert I; Marsmann M; Rosler C; Beck J; Nassal M, Involvement of the Host DNA-Repair Enzyme Tdp2 in Formation of the Covalently Closed Circular DNA Persistence Reservoir of Hepatitis B Viruses. Proc. Natl. Acad. Sci. USA 2014, 111, E4244–E4253. [PubMed: 25201958]

13. Maciejewski S; Nguyen JH; Gomez-Herreros F; Cortes-Ledesma F; Caldecott KW; Semler BL, Divergent Requirement for a DNA Repair Enzyme During Enterovirus Infections. MBio 2015, 7, e01931–15. [PubMed: 26715620]

14. Virgen-Slane R; Rozovics JM; Fitzgerald KD; Ngo T; Chou W; van der Heden van Noort GJ; Filippov DV; Gershon PD; Semler BL, An Rna Virus Hijacks an Incognito Function of a DNA Repair Enzyme. Proc. Natl. Acad. Sci. USA 2012, 109, 14634–14639. [PubMed: 22908287]

15. Raoof A; Depledge P; Hamilton NM; Hamilton NS; Hitchin JR; Hopkins GV; Jordan AM; Maguire LA; McGonagle AE; Mould DP; Rushbrooke M; Small HF; Smith KM; Thomson GJ; Turlais F; Waddell ID; Waszkowycz B; Watson AJ; Ogilvie DJ, Toxoflavins and Deazaflavins as the First Reported Selective Small Molecule Inhibitors of Tyrosyl-DNA Phosphodiesterase II. J. Med. Chem 2013, 56, 6352–6370. [PubMed: 23859074]

16. Kont YS; Dutta A; Mallisetty A; Mathew J; Minas T; Kraus C; Dhopeshwarkar P; Kallakury B; Mitra S; Uren A; Adhikari S, Depletion of Tyrosyl DNA Phosphodiesterase 2 Activity Enhances Etoposide-Mediated Double-Strand Break Formation and Cell Killing. DNA Repair 2016, 43, 38–47. [PubMed: 27235629]

17. Kankanala J; Marchand C; Abdelmalak M; Aihara H; Pommier Y; Wang ZQ, Isoquinoline-1,3-Diones as Selective Inhibitors of Tyrosyl DNA Phosphodiesterase II (Tdp2). J. Med. Chem 2016, 59, 2734–2746. [PubMed: 26910725]

18. Hornyak P; Askwith T; Walker S; Komulainen E; Paradowski M; Pennicott LE; Bartlett EJ; Brissett NC; Raoof A; Watson M; Jordan AM; Ogilvie DJ; Ward SE; Atack JR; Pearl LH; Caldecott KW; Oliver AW, Mode of Action of DNA-Competitive Small Molecule Inhibitors of Tyrosyl DNA Phosphodiesterase 2. Biochem. J 2016, 473, 1869–1879. [PubMed: 27099339]

19. Marchand C; Abdelmalak M; Kankanala J; Huang SY; Kiselev E; Fesen K; Kurahashi K; Sasanuma H; Takeda S; Aihara H; Wang ZQ; Pommier Y, Deazaflavin Inhibitors of Tyrosyl-DNA Phosphodiesterase 2 (Tdp2) Specific for the Human Enzyme and Active against Cellular Tdp2. ACS Chem. Biol 2016, 11, 1925–1933. [PubMed: 27128689]

20. Kossmann BR; Abdelmalak M; Lopez S; Tender G; Yan C; Pommier Y; Marchand C; Ivanov I, Discovery of Selective Inhibitors of Tyrosyl-DNA Phosphodiesterase 2 by Targeting the Enzyme DNA-Binding Cleft. Bioorg. Med. Chem. Lett 2016, 26, 3232–3236. [PubMed: 27262595]

21. Ribeiro CJA; Kankanala J; Shi K; Kurahashi K; Kiselev E; Ravji A; Pommier Y; Aihara H; Wang ZQ, New Fluorescence-Based High-Throughput Screening Assay for Small Molecule Inhibitors of Tyrosyl-DNA Phosphodiesterase 2 (Tdp2). Eur. J. Pharm. Sci 2018, 118, 67–79. [PubMed: 29574079]

22. Ribeiro CJA; Kankanala J; Xie J; Williams J; Aihara H; Wang Z, Triazolopyrimidine and Triazolopyridine Scaffolds as Tdp2 Inhibitors. Bioorg. Med. Chem. Lett 2019, 29, 257–261. [PubMed: 30522956]

23. Beck DE; Lv W; Abdelmalak M; Plescia CB; Agama K; Marchand C; Pommier Y; Cushman M, Synthesis and Biological Evaluation of New Fluorinated and Chlorinated Indenoisoquinoline Topoisomerase I Poisons. Bioorg. Med. Chem 2016, 24, 1469–1479. [PubMed: 26906474]

24. Wang P; Elsayed MSA; Plescia CB; Ravji A; Redon CE; Kiselev E; Marchand C; Zeleznik O; Agama K; Pommier Y; Cushman M, Synthesis and Biological Evaluation of the First Triple Inhibitors of Human Topoisomerase 1, Tyrosyl-DNA Phosphodiesterase 1 (Tdp1), and Tyrosyl-DNA Phosphodiesterase 2 (Tdp2). J. Med. Chem 2017, 60, 3275–3288. [PubMed: 28418653]

25. Yu L-M; Hu Z; Chen Y; Ravji A; Lopez S; Plescia CB; Yu Q; Yang H; Abdelmalak M; Saha S; Agama K; Kiselev E; Marchand C; Pommier Y; An L-K, Synthesis and Structure-Activity Relationship of Furoquinolinediones as Inhibitors of Tyrosyl-DNA Phosphodiesterase 2 (Tdp2). Eur. J. Med. Chem 2018, 151, 777–796. [PubMed: 29677635]

26. Laev SS; Salakhutdinov NF; Lavrik OI, Tyrosyl-DNA Phosphodiesterase Inhibitors: Progress and Potential. Bioorg. Med. Chem 2016, 24, 5017–5027. [PubMed: 27687971]

27. Baell JB; Holloway GA, New Substructure Filters for Removal of Pan Assay Interference Compounds (Pains) from Screening Libraries and for Their Exclusion in Bioassays. J. Med. Chem 2010, 53, 2719–2740. [PubMed: 20131845]

28. Chan DMT; Monaco KL; Li RH; Bonne D; Clark CG; Lam PYS, Copper Promoted C-N and C-O Bond Cross-Coupling with Phenyl and Pyridylboronates. Tetrahedron Lett. 2003, 44, 3863–3865.

29. Chan DMT; Monaco KL; Wang RP; Winters MP, New N- and O-Arylations with Phenylboronic Acids and Cupric Acetate. Tetrahedron Lett. 1998, 39, 2933–2936.

30. Lam PYS; Clark CG; Saubern S; Adams J; Winters MP; Chan DMT; Combs A, New Aryl/ Heteroaryl C-N Bond Cross-Coupling Reactions Via Arylboronic Acid Cupric Acetate Arylation. Tetrahedron Lett. 1998, 39, 2941–2944.

31. Siva Reddy A; Ranjith Reddy K; Nageswar Rao D; Jaladanki CK; Bharatam PV; Lam PY; Das P, Copper(Ii)-Catalyzed Chan-Lam Cross-Coupling: Chemoselective N-Arylation of Aminophenols. Org. Biomol. Chem 2017, 15, 801–806. [PubMed: 28045171]

32. Vernekar SKV; Tang J; Wu B; Huber AD; Casey MC; Myshakina N; Wilson DJ; Kankanala J; Kirby KA; Parniak MA; Sarafianos SG; Wang Z, Double-Winged 3-Hydroxypyrimidine-2,4-Diones: Potent and Selective Inhibition against HIV-1 RNase H with Significant Antiviral Activity. J. Med. Chem 2017, 60, 5045–5056. [PubMed: 28525279]

33. Wu B; Tang J; Wilson DJ; Huber AD; Casey MC; Ji J; Kankanala J; Xie J; Sarafianos SG; Wang Z, 3-Hydroxypyrimidine-2,4-Dione-5-N-Benzylcarboxamides Potently Inhibit HIV-1 Integrase and RNase H. J. Med. Chem 2016, 59, 6136–6148. [PubMed: 27283261]

34. Kansy M; Senner F; Gubernator K, Physicochemical High Throughput Screening: Parallel Artificial Membrane Permeation Assay in the Description of Passive Absorption Processes. J. Med. Chem 1998, 41, 1007–1010. [PubMed: 9544199]

35. Zafrani Y; Yeffet D; Sod-Moriah G; Berliner A; Amir D; Marciano D; Gershonov E; Saphier S, Difluoromethyl Bioisostere: Examining the "Lipophilic Hydrogen Bond Donor" Concept. J. Med. Chem 2017, 60, 797–804. [PubMed: 28051859]

36. Mabit H; Dubanchet S; Capel F; Dauguet C; Petit MA, In-Vitro Infection of Human Hepatoma-Cells (HepG2) with Hepatitis-B Virus (HBV) - Spontaneous Selection of a Stable HBV Surface Antigen-Producing HepG2 Cell-Line Containing Integrated HBV DNA-Sequences. J. Gen. Virol 1994, 75, 2681–2689. [PubMed: 7931154]

37. Terasaki K; Hirayama H; Kasanga CJ; Maw MT; Ohya K; Yamaguchi T; Fukushi H, Chicken B Lymphoma Dt40 Cells as a Useful Tool for in Vitro Analysis of Pathogenic Infectious Bursal Disease Virus. J. Vet. Med. Sci 2008, 70, 407–410. [PubMed: 18460838]

38. Kumar K; Woo SM; Siu T; Cortopassi WA; Duarte F; Paton RS, Cation-Pi Interactions in Protein-Ligand Binding: Theory and Data-Mining Reveal Different Roles for Lysine and Arginine. Chem. Sci 2018, 9, 2655–2665. [PubMed: 29719674]

39. Gallivan JP; Dougherty DA, Cation-Pi Interactions in Structural Biology. Proc. Natl. Acad. Sci. USA 1999, 96, 9459–9464. [PubMed: 10449714]

40. Ma JC; Dougherty DA, The Cation–Π Interaction. Chem. Rev 1997, 97, 1303–1324. [PubMed: 11851453]

41. Minoux H; Chipot C, Cation-Pi Interactions in Proteins: Can Simple Models Provide an Accurate Description? J. Am. Chem. Soc 1999, 121, 10366–10372.

42. Zacharias N; Dougherty DA, Cation-Pi Interactions in Ligand Recognition and Catalysis. Trends Pharmacol. Sci 2002, 23, 281–287. [PubMed: 12084634]

43. Wintjens R; Lievin J; Rooman M; Buisine E, Contribution of Cation-Pi Interactions to the Stability of Protein-DNA Complexes. J. Mol. Biol 2000, 302, 395–410. [PubMed: 10970741]

44. Evans DA; Katz JL; West TR, Synthesis of Diaryl Ethers through the Copper-Promoted Arylation of Phenols with Arylboronic Acids. An Expedient Synthesis of Thyroxine. Tetrahedron Lett. 1998, 39, 2937–2940.

45. Chen XX; Murawski A; Patel K; Crespi CL; Balimane PV, A Novel Design of Artificial Membrane for Improving the Pampa Model. Pharm. Res 2008, 25, 1511–1520. [PubMed: 18185985]

46. Mosmann T, Rapid Colorimetric Assay for Cellular Growth and Survival: Application to Proliferation and Cytotoxicity Assays. J. Immunol. Methods 1983, 65, 55–63. [PubMed: 6606682]

47. Schrödinger Small-Molecule Drug Discovery Suite 2015–4, Schrödinger, Llc, New York, Ny, 2015.

48. Sastry GM; Adzhigirey M; Day T; Annabhimoju R; Sherman W, Protein and Ligand Preparation: Parameters, Protocols, and Influence on Virtual Screening Enrichments. J. Comput. Aid. Mol. Des 2013, 27, 221–234.

49. Schrödinger Schrödinger Release 2015–4: Schrödinger Suite 2015–4 (a)Protein Preparation Wizard; Epik, Schrödinger, Llc, New York, Ny, 2015; Impact, Schrödinger, Llc, New York, Ny, 2015; Prime, Schrödinger, Llc, New York, Ny, 2015.

50. Jorgensen WL; Maxwell DS; TiradoRives J, Development and Testing of the OPLS All-Atom Force Field on Conformational Energetics and Properties of Organic Liquids. J. Am. Chem. Soc 1996, 118, 11225–11236.

51. Schrödinger Schrödinger Release 2015–4: Schrödinger Suite 2015–4 (a)Protein Preparation Wizard; Epik, Schrödinger, Llc, New York, Ny, 2015; Impact, Schrödinger, Llc, New York, Ny, 2015; Prime, Schrödinger, Llc, New York, Ny, 2015.

52. Schrödinger Schrödinger Release 2015–4: Ligprep, Schrödinger, Llc, New York, Ny, 2015.

53. Friesner RA; Murphy RB; Repasky MP; Frye LL; Greenwood JR; Halgren TA; Sanschagrin PC; Mainz DT, Extra Precision Glide: Docking and Scoring Incorporating a Model of Hydrophobic Enclosure for Protein-Ligand Complexes. J. Med. Chem 2006, 49, 6177–6196. [PubMed: 17034125]

54. Release Schrödinger 2015–4: Glide Version 6.9, Schrödinger, Llc, New York, Ny, 2015.
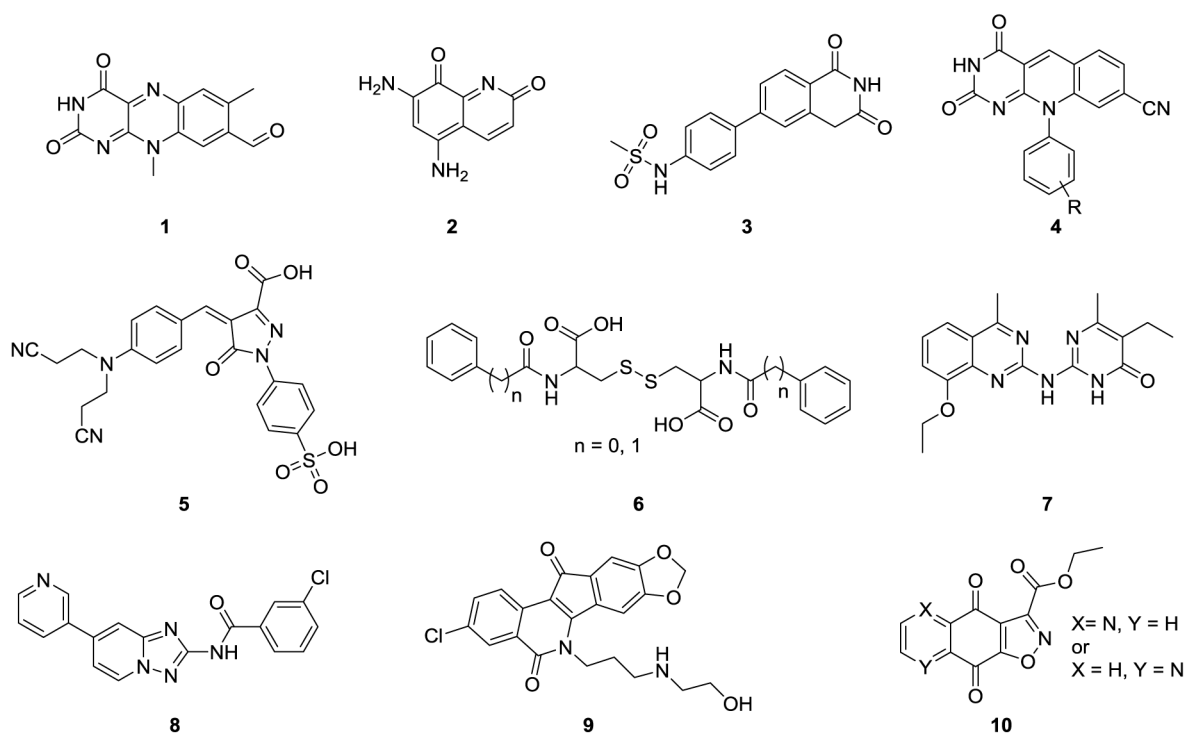
Figure 1.
Reported TDP2 inhibitors. Deazaflavin **4** is the most potent and best characterized TDP2 inhibitor type.
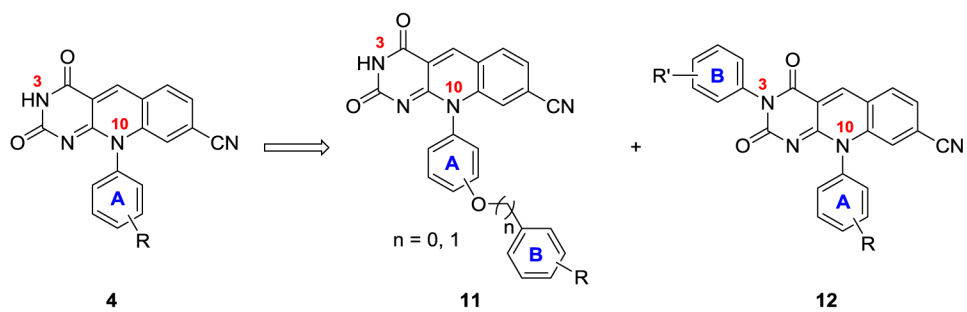
Figure 2.
Novel deazaflavin subtypes **11**-**12** designed to improve lipophilicity by adding a second phenyl ring (B) directly off ring A (for subtype **11**) or at N-3 site (for subtype **12**).
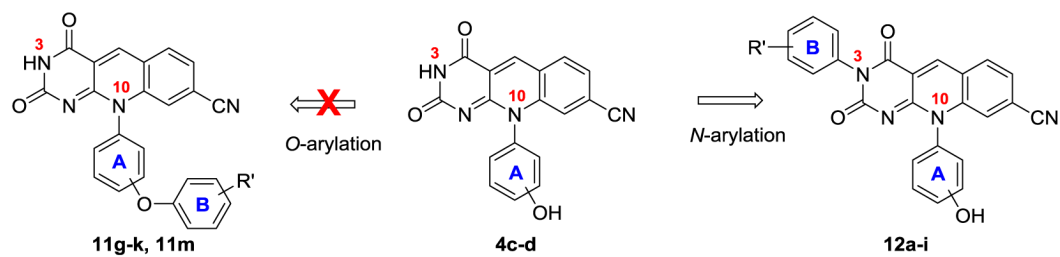
Figure 3.
Chemoselectivity of the Chan-Lam coupling reaction. Under reaction conditions, the arylation occurred exclusively at the *N*-3 site to yield subtype **12** with *O*-arylated products **11** not observed.
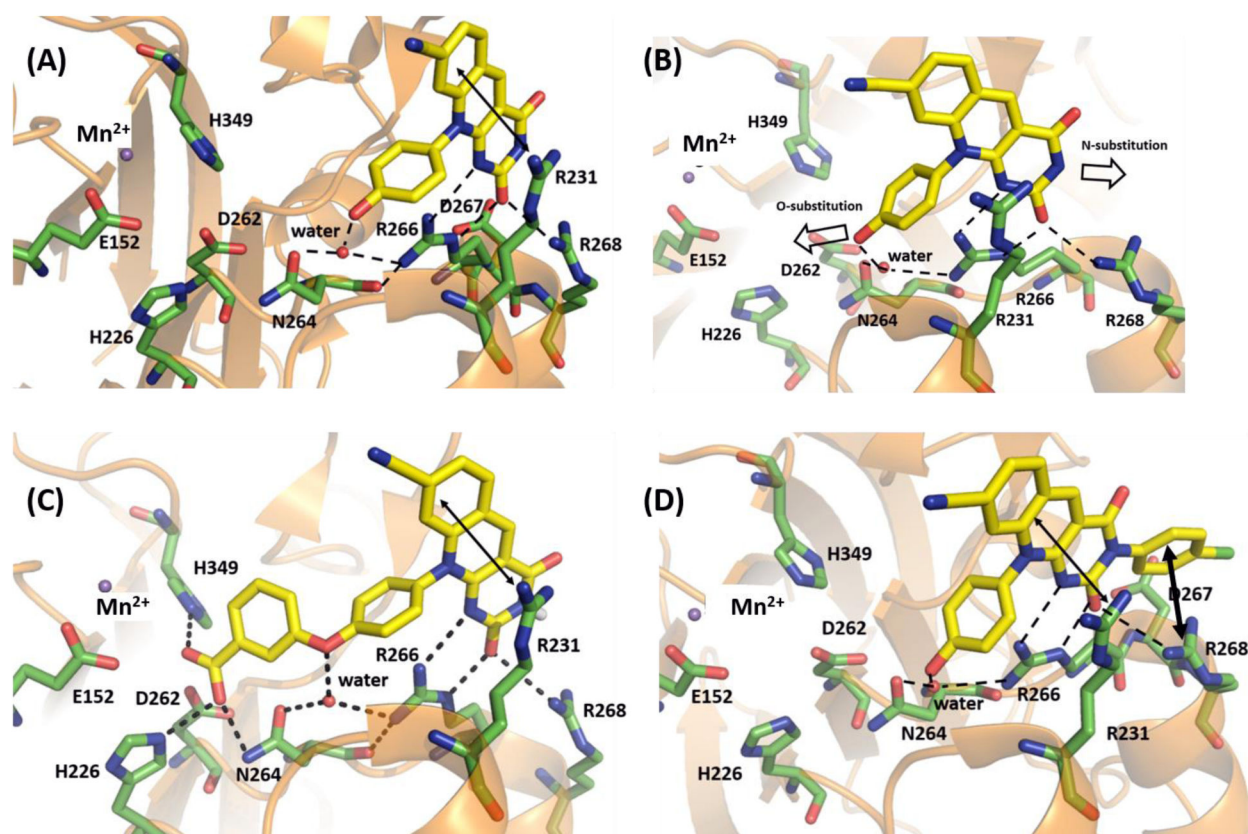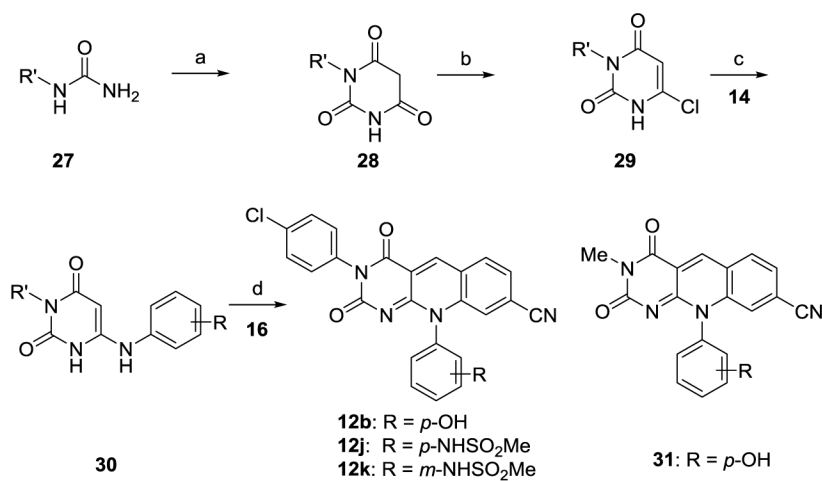
Figure 5.
Molecular modeling of **11k** and **12b**. (A) Binding mode of **4c** within the crystal structure of catalytic domain of humanized mouse TDP2 (PDB code: 5J42[18]). (B) Potential vectors for designing novel deazaflavin inhibitor types. (C) Predicted binding mode of **11k** within the catalytic domain of humanized mouse TDP2. (D) Predicted binding mode of **12b** within the catalytic domain of humanized mouse TDP2. Key residues are highlighted in green sticks. H-bond interactions are depicted as black dotted lines. Cation-π and π-π interaction are represented as double headed arrow in black. Water molecule and magnesium ion were represented as red and blue non-bonded sphere. All the residue numberings are based on the human TDP2.
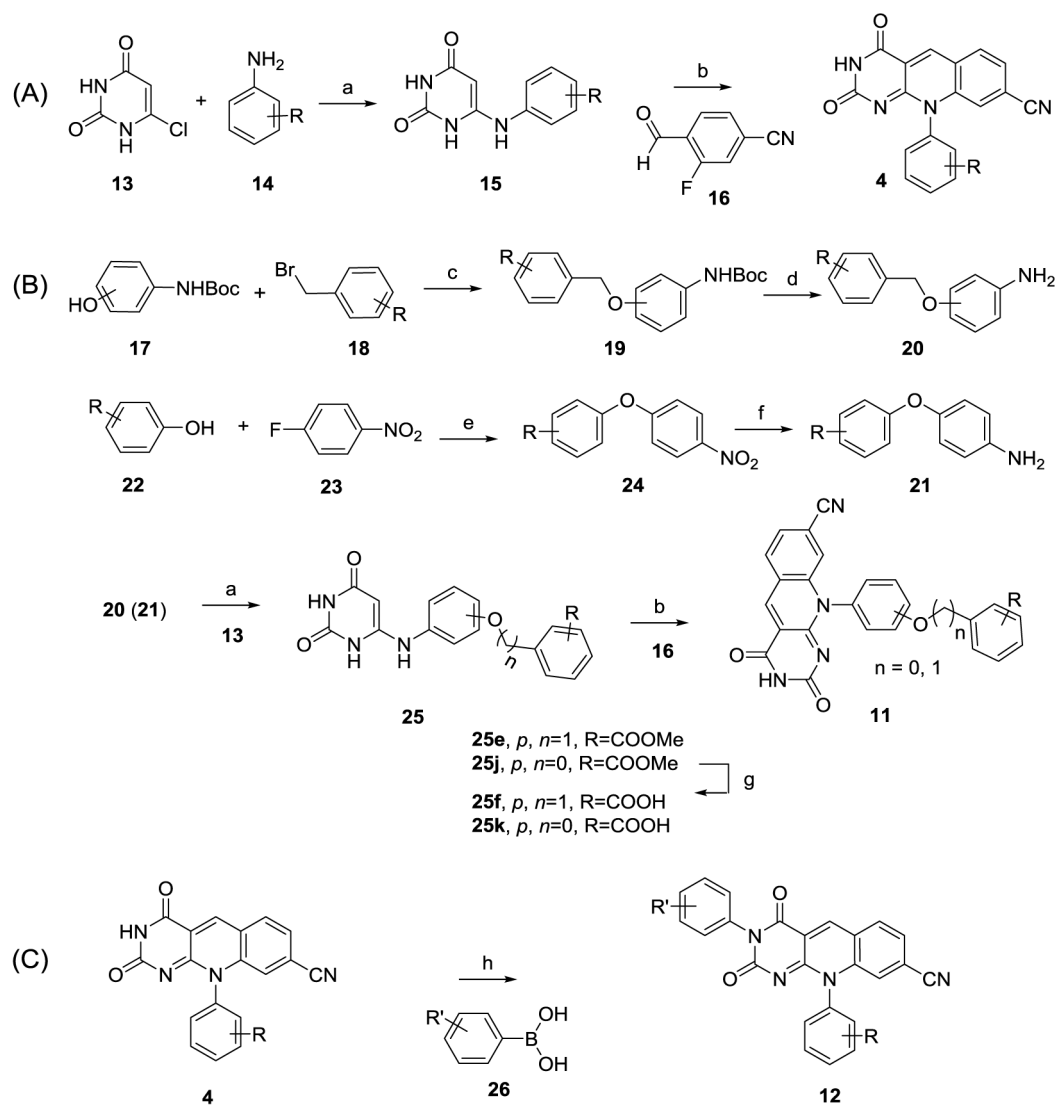
Scheme 1.
Synthesis of deazaflavin scaffold **4** and new subtypes **11-12**

[a]Reagents and conditions: a) EtOH, 150 °C, 30 min, MW, 60–85%; b) DMF, 110 °C, MW, 30 min, 40–60%; c) K$_2$CO$_3$, DMF, r. t., 12 h; d) TFA, DCM, r. t., 6h, 60–75% over two steps; e) K$_2$CO$_3$, DMF, 110°C, 12h, 59%; f) 10% Pd/C, EtOAc, rt, o. n. 87%; g) EtOH, NaOH 1N, reflux, 3h, 85% h) Cu(OAc)$_2$, DMF, air, r. t., 24–48 h, 40–52%.

Scheme 2.
Alternative linear synthesis for subtype **12**

[a]Reagents and conditions: a) Diethylmalonate, NaOEt, EtOH, reflux, o. n., 86%; b) POCl$_3$, BnEt$_3$NCl, 50 °C, 6 h, 70%; c) aniline derivative, EtOH, 150 °C, 30 min, MW, 55–80%; d) DMF, 110 °C, 30 min, MW, 50–69%.
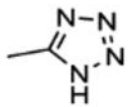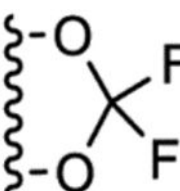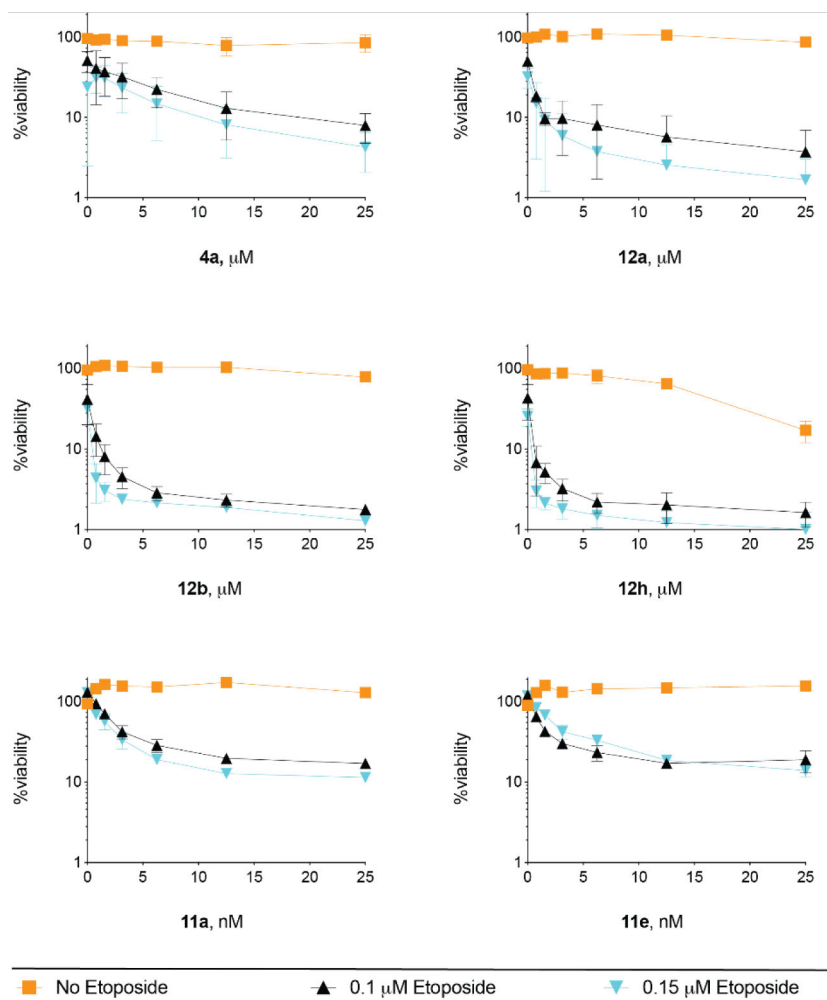
Figure 4.
Effect of TDP2 inhibitors **4a**, **12a**, **12b**, **12h**, **11a** and **11e** on potentiating toxic action of ETP.

Table 1.

TDP2 inhibitory activity and PAMPA permeability for the control series.
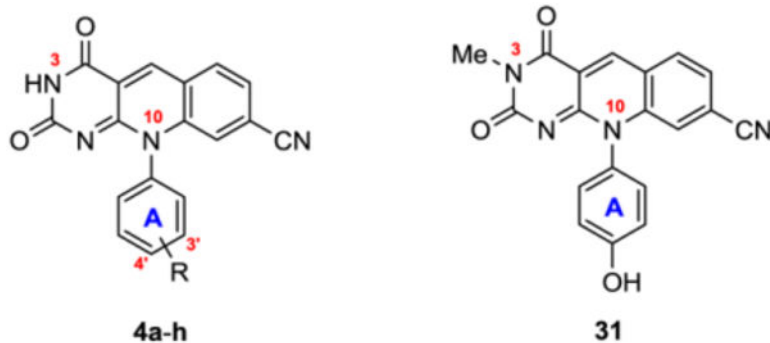
Compd	R		TDP2 IC$_{50}$ (μM)^{a}	PAMPA P$_{e}$ (10^{-6} cm/s)^{b}
4a^{c}	3′	(tetrazole)	0.041 ± 0.003	0.003
4b^{c}		3′ OH	0.042 ± 0.004	0.01
4c^{c}		4′ OH	0.14 ± 0.01	0.008
4d^{c}		H	0.64 ± 0.02	0.4
4e		4′ OCF$_{3}$	1.0 ± 0.1	1.1
4f		4′ OCHF$_{2}$	0.88 ± 0.06	0.3
4g		(dioxolane)	0.96 ± 0.02	0.5
4h		(difluorodioxolane)	1.5 ± 0.1	1.1
31		--	0.32 ± 0.02	0.1

^{a}IC$_{50}$: concentration of a compound producing 50% inhibition, expressed as mean ± standard deviation from three independent experiments performed in triplicate.

[b] P_e: effective permeability coefficients determined using the PAMPA, measured in five replicates.

[c] Previously reported analogues. Reported IC_{50} values are 0.04 μM (**4a**), 0.05 μM (**4b**), 0.09 μM (**4c**) and 0.50 μM (**4d**).[15]

Table 2.

TDP2 inhibitory activity, PAMPA permeability and cytotoxicity for analogues from phenolic OH modifications (**11a-m**).

Compd	R	TDP2 IC$_{50}$ (μM)[a]	PAMPA P$_e$ (10^{-6} cm/s)[b]
4c	--	0.14 ± 0.01	0.008
11a	H	0.20 ± 0.02	1.2
11b	4′ Cl	1.6 ± 0.2	0.4
11c	4′ Br	1.3 ± 0.0	0.2
11d	3′ Cl	0.99 ± 0.09	0.4
11e	3′ CO$_2$Me	0.15 ± 0.01	0.6
11f	3′ CO$_2$H	0.13 ± 0.01	0.01
11g	H	1.1 ± 0.1	2.8
11h	4′ Cl	>10	0.8
11i	4′ F	3.8 ± 0.3	2.7
11j	3′ CO$_2$Me	0.93 ± 0.05	0.7
11k	3′ CO$_2$H	0.19 ± 0.01	0.003
4b	--	0.041 ± 0.004	0.01
11l	--	0.38 ± 0.02	1.7
11m	--	0.30 ± 0.00	2.0

[a]IC$_{50}$: concentration of a compound producing 50% inhibition, expressed as mean ± standard deviation from three independent experiments performed in triplicate.

[b]P$_e$: effective permeability coefficients determined using the PAMPA, measured in five replicates.

Table 3.

TDP2 inhibitory activity and PAMPA permeability for analogues from N-3 modifications (**12a-i**).

12a-f   12g-i
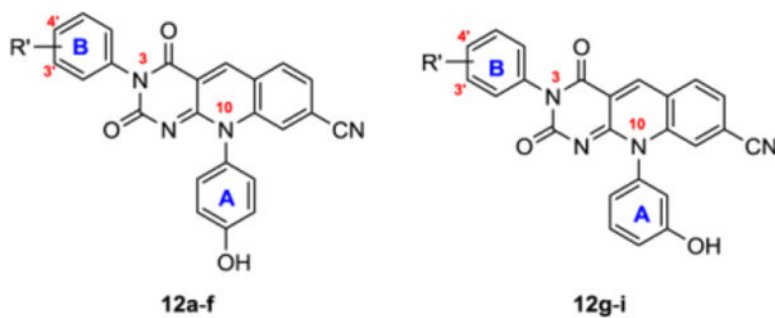
Compd	R′	TDP2 IC$_{50}$ (μM)[a]	PAMPA P$_e$ (10^{-6} cm/s)[b]
4c	--	0.14 ± 0.01	0.008
12a	H	0.033 ± 0.001	0.1
12b	4′ Cl	0.033 ± 0.002	0.08
12c	4′ F	0.070 ± 0.003	0.06
12d	4′ Br	0.065 ± 0.003	0.05
12e	3′ CO$_2$Me	0.038 ± 0.003	0.03
12f	3′ CONH$_2$	0.035 ± 0.000	0.01
4b	--	0.042 ± 0.004	0.01
12g	4′ Cl	0.0073 ± 0.0003	0.04
12h	3′ Cl	0.020 ± 0.002	0.07
12i	3′, 4′ di-Cl	0.014 ± 0.000	0.03

[a]IC$_{50}$: concentration of a compound producing 50% inhibition, expressed as mean ± standard deviation from three independent experiments performed in triplicate.

[b]P$_e$: effective permeability coefficients determined using the PAMPA, measured in five replicates.

Table 4.

TDP2 inhibitory activity and PAMPA permeability for additional analogues of subtype **12** with N-10 phenyl A modifications.
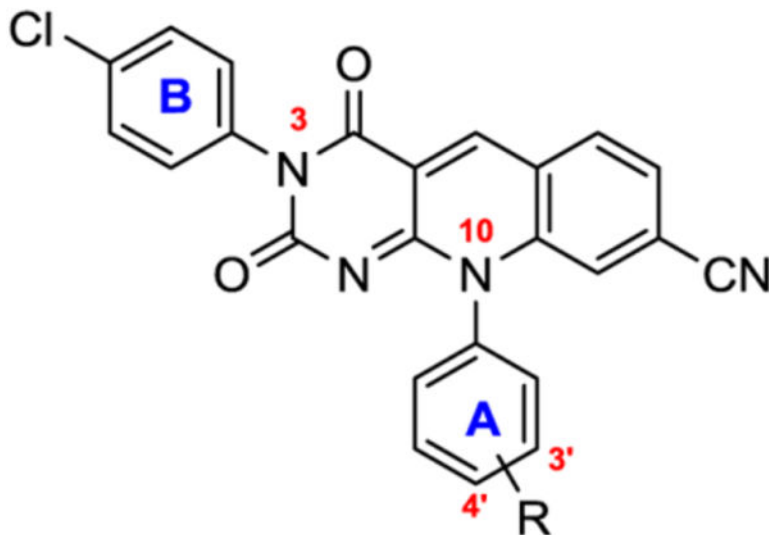
Compd	R	TDP2 IC$_{50}$ (μM)^a	PAMPA P$_e$ (10^{-6} cm/s)^b
12b	4′ OH	0.033 ± 0.002	0.08
12j	4′ NHSO$_2$Me	0.0065 ± 0.0004	0.02
12g	3′ OH	0.0073 ± 0.0003	0.04
12k	3′ NHSO$_2$Me	0.0061 ± 0.0006	0.06
12l	H	0.27 ± 0.02	4.4

^{a}IC$_{50}$: concentration of a compound producing 50% inhibition, expressed as mean ± standard deviation from three independent experiments performed in triplicate.

^{b}P$_e$: effective permeability coefficients determined using the PAMPA, measured in five replicates.

Table 5.

Cytotoxicity evaluation in two cell lines.

Compd	CC_{50} (μM)[a]		PAMPA P_e (10^{-6} cm/s)[b]	Compd	CC_{50} (μM)[a]		PAMPA P_e (10^{-6} cm/s)[b]
	HepG2	HeLa			HepG2	HeLa	
4a[d]	>100	>100	0.003	**11i**	14	12	2.7
4b[d]	>100	--	0.01	**11j**	8.7	9.4	0.7
4c[d]	>100	--	0.008	**11k**	>100	>100	0.003
4d[d]	>100	--	0.4	**11l**	25	30	1.7
4e	40	28	1.1	**11m**	9.0	21	2.0
4f	85	79	0.3	**12a**	50	>100	0.1
4g	>100	>100	0.5	**12b**	41	45	0.08
4h	42	39	1.1	**12c**	46	32	0.06
31	>100	>100	0.1	**12d**	49	67	0.05
11a	14	12	1.2	**12e**	>100	--	0.03
11b	>100	>100	0.4	**12f**	>100	--	0.01
11c	17	--	0.2	**12g**	85	65	0.04
11d	14	12	0.4	**12h**	82	90	0.07
11e	29	29	0.6	**12i**	42	62	0.03
11f	>100	>100	0.01	**12j**	>100	>100	0.02
11g	29	--	2.8	**12k**	>100	>100	0.06
11h	5.3	7.4	0.8	**12l**	33	25	4.4

[a]CC_{50}: concentration of a compound causing 50% cell death. ETP was used as control: CC_{50} = 15 μM (HepG2) and 17 μM (HeLa).

[b]P_e: effective permeability coefficients determined using the PAMPA, measured in five replicates.

Table 6.

TDP2 inhibitory activity, permeability and cytotoxicity profiles of selected analogues.

Compd	TDP2 IC$_{50}$ (μM)^a	PAMPA P$_e$ (10^{-6} cm/s)^b	CC$_{50}$ (μM)^c	
			HepG2	HeLa
11a	0.20 ± 0.02	1.2	14	12
11e	0.15 ± 0.01	0.6	29	29
12a	0.033 ± 0.001	0.1	50	>100
12b	0.033 ± 0.002	0.08	41	45
12g	0.0073 ± 0.0003	0.04	85	65
12h	0.020 ± 0.002	0.07	82	90
12j	0.0065 ± 0.0004	0.02	>100	>100
12k	0.0061 ± 0.0006	0.06	>100	>100
4a^d	0.041 ± 0.003	0.003	>100	>100
4b^d	0.042 ± 0.004	0.01	>100	--
4c^d	0.14 ± 0.01	0.008	>100	--

^{a}IC$_{50}$: concentration of a compound producing 50% inhibition, expressed as mean ± standard deviation from three independent experiments.

^{b}P$_e$: effective permeability coefficients determined using the PAMPA, measured in five replicates.

^{c}CC$_{50}$: concentration of a compound causing 50% cell death.

^{d}Previously reported[15] analogues.